Activity and stability of nanosized SAPO-34 in the reaction of methanol to olefins

PROYECTO FINAL MÁSTER QUÍMICA SOSTENIBLE

Presentado por: Zhibin Li

Dirigido por:

Prof. Avelino Corma Canós

Dr. Joaquín Martínez Triguero

Acknowledgements

First I offer my sincerest gratitude to my supervisors, Professor Avelino Corma and Doctor Joaquin Martinez, who have supported me throughout my thesis with their patience and knowledge. Without their help, I would not finish the master study.

And I also want to thank Professor Jihong Yu from my home university Jilin University. Professors Yu and Avelino offer me the opportunity to study in ITQ, and also for their support.

Thanks for the help from the people in ITQ, they give me a lot of help not only in my study and but also in the daily life.

I thank China Scholarship Council (CSC) for supporting me throughout all my studies in Spain, which offer me the grant to finish my Ph D.

Finally I want to thank my parents and my wife for their support and encourage.

Index

1. Introduction....1

1.1 Zeolites....1

1.2 Methanol to olefin (MTO)....3

1.3 Mechanism of MTO....4

1.4 Objective of the study and precedents....9

2. Experimental....13

2.1 Synthesis of materials....13

2.2 Characterization....14

2.3 Methanol to Olefin test....15

3 Results and discussion....16

3.1 XRD and Microscopy....16

3.2 N_2 Adsorption....23

3.4 FTIR and CO Adsorption....29

3.5 Methanol to hydrocarbons activity....33

3.6 Stabilization of nanoSAPO-34 by hydrothermal treatment....41

4. Conclusions....45

5. References....46

1. Introduction

1.1 Zeolites

Zeolites are a kind of porous material, which are widely used in industry, such as oil cracking and fine chemistry because of the remarkable properties of activity and selectivity.[1]

Zeolites have a unique system of channels and cavities, which make them different with other materials[2]. Their structures are built with the tetrahedral units TO_4 (T= Si, Al), which are in a three-dimensional array, and the tetrahedral units are connect with a common oxygen atom. From the IUPAC, a classification can be done for three types because of the pore sizes: micropores: (2.0 nm≥dp), mesopores: 2.0nm< dp≤d 50 nm, macropores: dp > 50 nm.

But zeolites obtained from natural can't be used directly, the reasons are as below: (1) they always contain other impurity phases (2) chemistry composition changes (3) not optimize the properties in catalysis application.[3]. Barrer and Milton got the first synthesized zeolite in the lab in 1950s, and since then scientists have got more than 200 kinds of zeolite frameworks from synthesis[4].

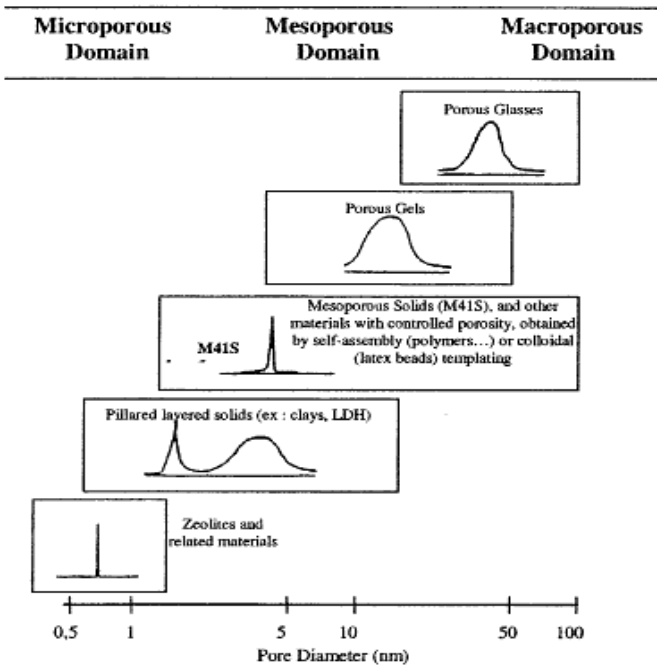

Fig 1 Examples of micro-, meso-, and macroporous materials, showing pore size domains and typical

pore size distributions[2].

One of the unique properties of zeolites is the selectivity in the chemistry reactions and can be described as below[5]:

Reactant-Shape Selectivity

When there are more than two reactants in the reactions, only the one whose size is smaller than zeolites pores can be allowed to entry the molecular channels, this kind of selectivity is called reactant-shape selectivity, as show in Fig 2[5]

Product-Shape Selectivity

When the reactions start, there may be different thermodynamically feasible products, but the potential products whose size is larger cannot diffuse from the molecular pores, this kind of selectivity is called Product-Shape Selectivity, as show in Figure 2

Transition-State Shape Selectivity

When the micropore channel used as a confined reactor, it can impose steric geometry restriction on the transitions state, this kind of selectivity is called Product-Shape Selectivity, as show in Figure 2 ,whose selectivity mostly depend not on crystal size or activity but on zeolite structure and pore diameter. Some newly studies show that electronic factor may play a important affection in shape-selective products, and they proposed a new concept named restricted-electronic transition-state selectivity [6, 7].

In 1962, faujasites (zeolites X and Y) were introduced to industry as the catalyst for fluid catalytic cracking (FCC) of heavy petroleum distillate, and it showed more activity and yield to compare with the catalyst used before in this process, this remarkable result attended more and more attention to the zeolites synthesis and its application in catalysis reactions[8]. Nowadays zeolites catalysts have been wildly used in fields of fine chemistry, agriculture, ion-exchange, and oil cracking, some of them are very important processes for our daily life.

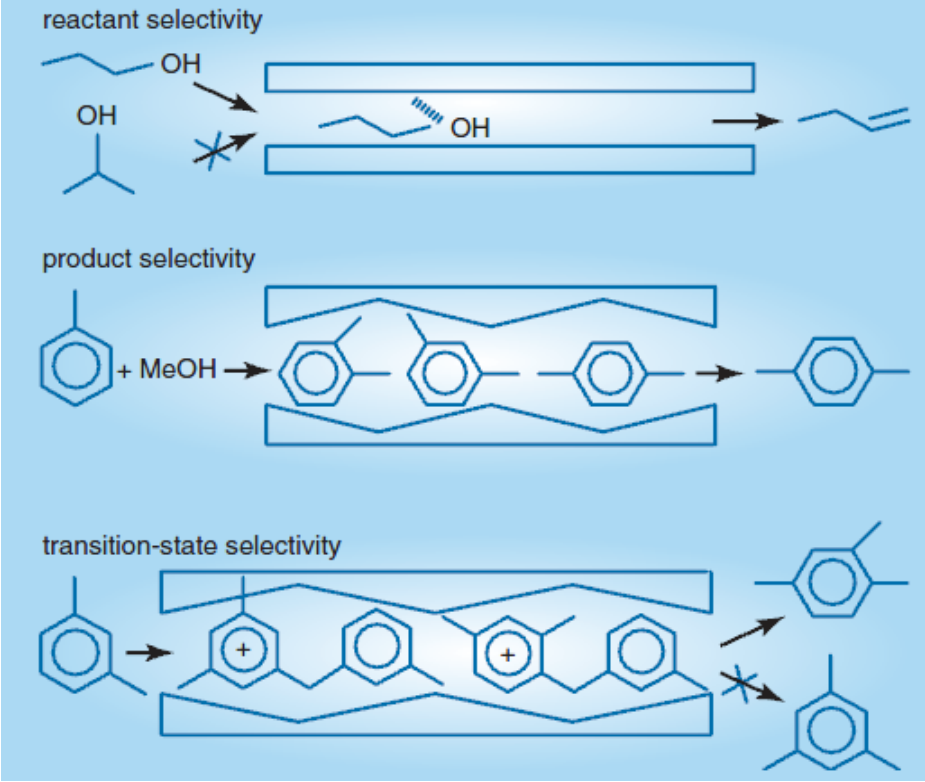

Fig 2 Three types of shape-selective catalytic reactions with representative examples: reactant-shape selectivity in the alcohol dehydration reactions; product shape selectivity in toluene methylation reactions; transition-state-shape selectivity in m-xylene disproportionation (transmethylation) reactions

1.2 Methanol to olefin (MTO)

Methanol to olefin is an important processes in industry for obtaining ethylene and propylene. It was discovered by the people from Mobil Central research when they tried to find new ways to get more gasoline from methanol and isobutene in 1970s [9]. Since then, a lot of researchers in world took their attention on the MTO studies. This process has not only economic but also scientific meaning to do more studies [10, 11], and also methanol can be processed catalytically to gasoline (methanol-to-gasoline, MTG), depending on operation conditions. Compared with the current ethylene and propylene production process such as steaming cracking of NGL and naphtha or other light fractions of petroleum, MTO offer a wider yield of ethylene and propylene to supply market needs. And at the same time methanol can be obtained from other sources of carbon-containing materials such as biomass and

natural gas, which is not easy to transform to conversion to ethylene and propylene directly [12, 13].

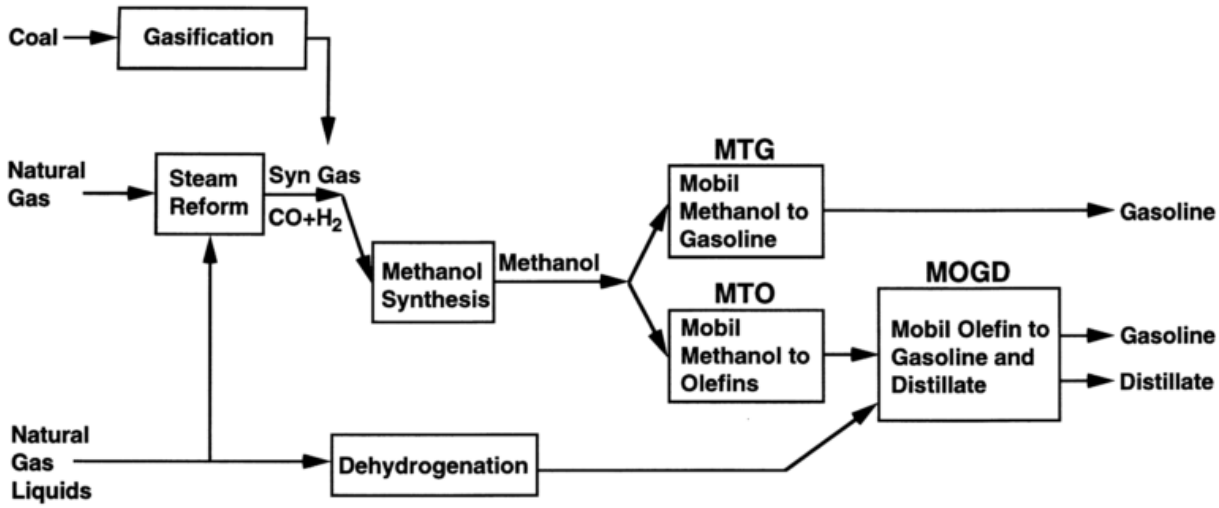

Fig. 3 Gasoline and distillate production via methanol and Mobil's ZSM-5 technology

1.3 Mechanism of MTO

The mechanism of MTO has been studied by plenty of scientists. According to the literature, the reaction can be divided to five stages[14]. First step is the equilibration among methanol dimethyl ether and water. Second, it is often called kinetic induction period on the fresh catalyst, which precedes high yield of hydrocarbon formed from methanol and dimethyl ether. The third, which is most important step, is the formation of initial hydrocarbon product. But about this part, there are so many questions to be answered: what is the first carbon product and how does it form? To answer this question, different scientist proposed more than 20 distinct mechanisms in these 40 years[11].

In figure 4 a and b, are the mechanism proposed by some researcher summary from the literatures, some of them thought CH_3+ or carbine: CH2 was formed when methanol was activated on the catalyst, each of them is shown in Fig. 4 a and b. And also some mechanisms which proposed methanol convert to a carbon-carbon bond species directly were summarized. Few free radical mechanisms also can be seen in the figure (shown in Fig 4 c).

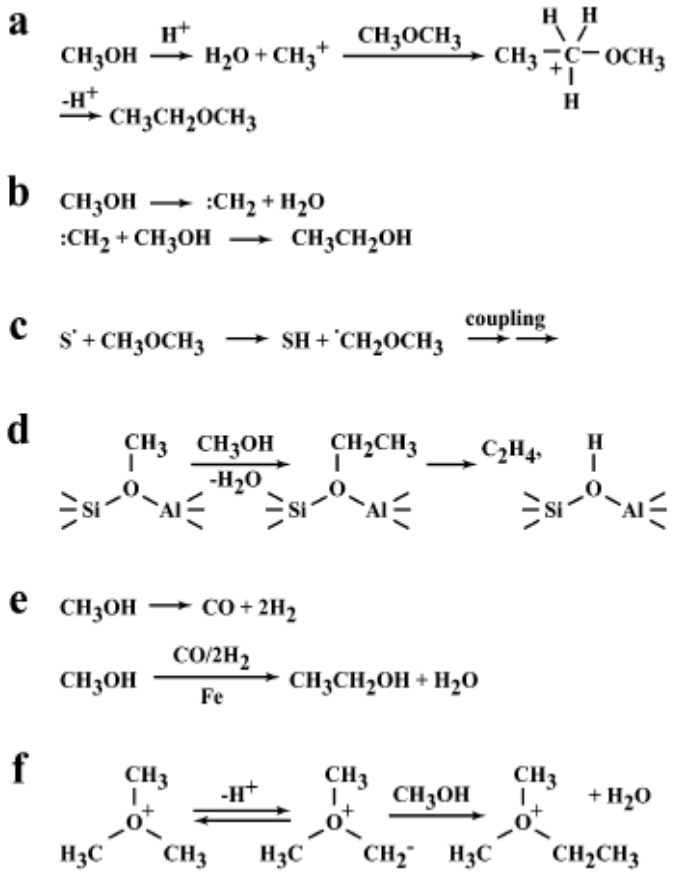

Fig 4 several of the classical "direct" mechanisms for the conversion of methanol/dimethyl ether to olefins (or a direct precursor) shown in highly abbreviated or conflated form: (a) A pathway showing a carbenium ion alkylating dimethyl ether to form a carbonium ion. (b) One of several proposed carbene pathways. (c) An abbreviation of one of several free radical routes. SO_2 is an unspecified surface radical species. (d) An alkoxy chain growth process occurring on a framework site. (e) One of the proposed mechanisms featuring CO, showing a role for transition-metal impurities. (f) An abbreviated oxonium-ylide route.[14]

Bound methoxy (methoxonium) species[15, 16] can be formed when methanol react with zeolite acid sites, but this kind of chain growth process for alkoxy(shown in Fig 4 d) has never been obtained in the experiments. And also one of the proposed mechanism thought the intermediate or cocatalyst in methanol conversion may be CO (shown in Fig 4 e), because small amount of CO appeared in the MTO and MTG reactors in the product gas. When CO was introduced to the reaction, there are no changes in reaction rate. To compare when label ^{13}CO was mixed with $^{12}CH_3OH$, there is no ^{13}C was found in the hydrocarbon products. There is no explanation about

the kinetic induction period in all of the above direct mechanisms. The reason may be the difficulty to find this and some researchers thought maybe there is a relatively inefficient direct mechanism functioned as “induction reaction “. And after the induction reaction, there may be more efficient auto catalysis reactions by olefin chain growth and cracking[17].

To more easily explain the primary product in the MTO reaction, the hydrocarbon pool routes have been proposed. The feature of this mechanism is that primary olefinic products and original hydrocarbon was got by a sequence of steps from the methanol reacted with entrained hydrocarbon species. There are some hydrocarbon pool ideas summarized in Figure 5[14]. In 1982 Mole and co-workers[18] and Langner[19] proposed an insightful MTO mechanism which led to a resolution of the MTO mechanism. (shown in figure 5 a and b)

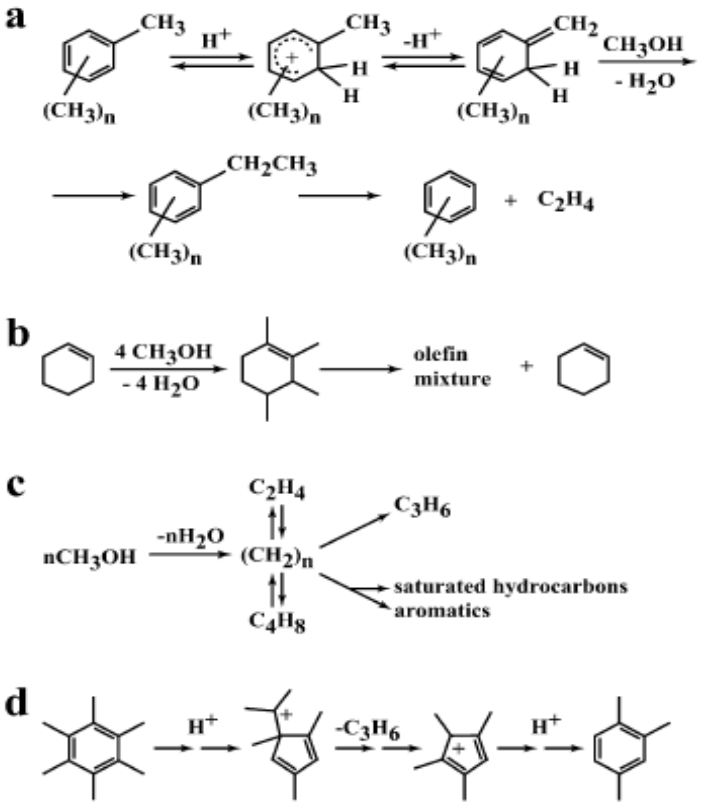

Fig 5 Early proposals that have significantly shaped current thinking about the hydrocarbon pool mechanism in MTO catalysis. (a) Mole’s 1983 mechanism of methylbenzene side-chain alkylation. (b) An abbreviated account of Langner’s explanation for the dramatic effect of cyclohexanol and other co-feeds of reducing the kinetic induction period. (c) Kolboe’s early phenomenological hydrocarbon pool mechanism for MTO catalysis. (d) The paring reaction in highly abbreviated form.

Kolboe proposed that olefins were formed from methanol reacting with a hydrocarbon pool of intermediates [20-22]as shown in Figure 5 c and his model was influenced by the earlier work.

Sullivan and co-workers [23] published a paper in 1961, in which he proposed “paring reaction”, this also rich the thinking of the MTO reaction mechanism right now.

And finally, in the last years it was shown that olefins are also part of the hydrocarbon pool, in which methanol alkylation of adsorbed C3+ olefins, with subsequent cracking are an important source of olefins as products in zeolite ZSM-5 and also in SAPO-34. Then, the combination of the aromatic and the olefin-based hydrocarbon pool is called the “dual cycle mechanism”[24-26].

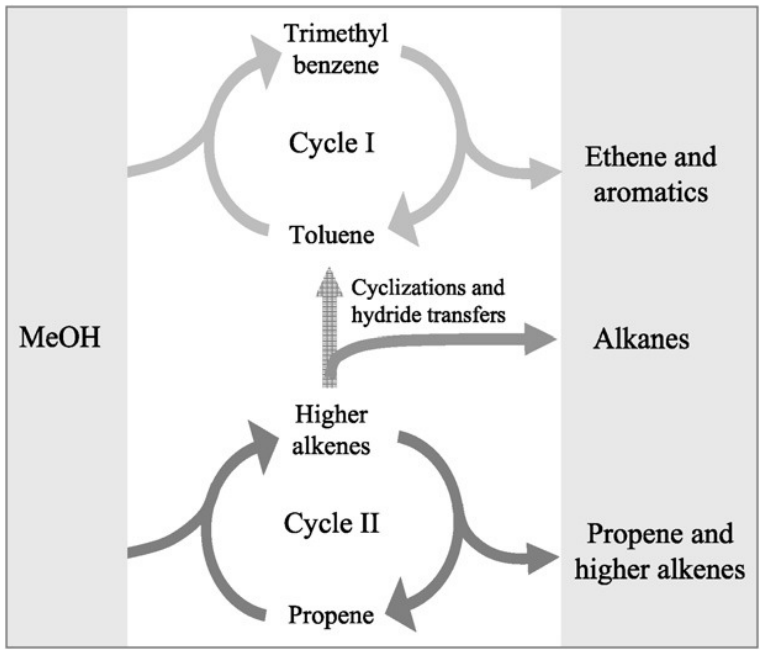

Fig 6. Dual cycle concept for the conversion of methanol on ZSM-5 (from ref [26]).

The fourth stage of methanol conversion catalysis is the conversion the primary olefin product to other hydrocarbons by the secondary reaction[14].And this kind of reaction is determined by zeolite acid strength ,crystallite size ,catalyst topology and acid site density, space velocity and other process condition.

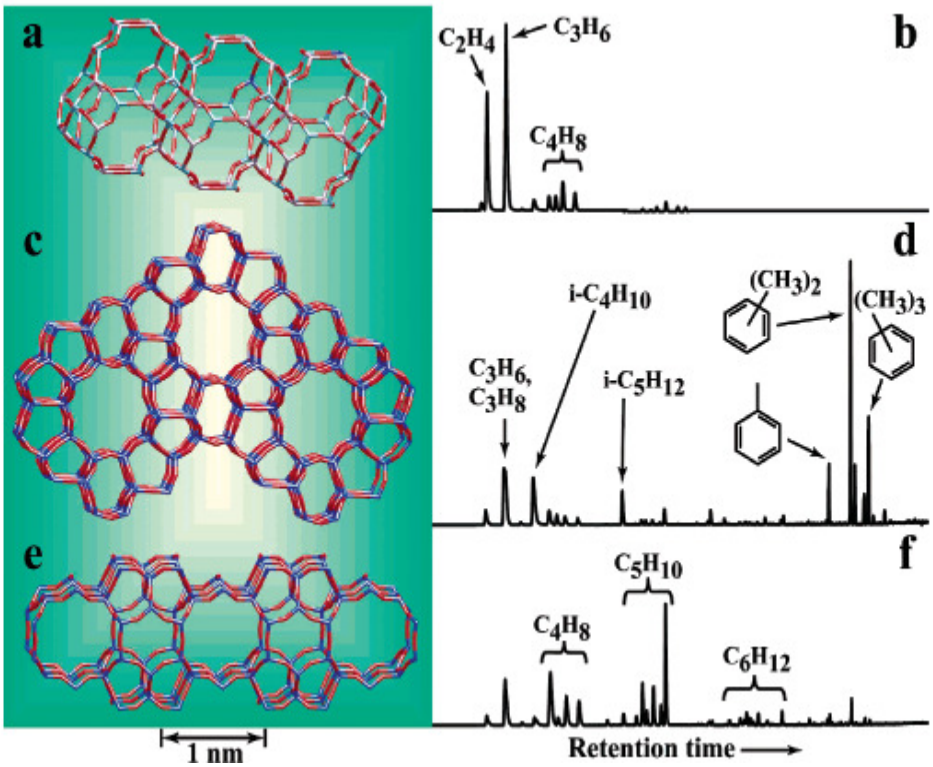

Fig 7 Three of the methanol conversion catalysts discussed in this contribution and GC-MS total ion chromatograms illustrating product selectivity on these materials: (a) The CHA topology of the silico-aluminophosphate catalyst HSAPO-34. (b) The products of methanol conversion on HSAPO-34. (c) The MFI structure of the aluminosilicate zeolite HZSM-5. (d) The products of methanol conversion on HZSM-5. (e) The FER topology of H-Ferrierite. (f) The products of methanol conversion on MTO catalysis on H-Ferrierite. Each experiment used 300 mg of catalyst operated at 723 K, and products were sampled 1.5 s following pulsed introduction of 10.2 μ L of methanol[14].

Figure 7 shows different structures for catalysts in MTO reaction and the corresponding products obtained by GC at 723 K. Fig 7 a SAPO-34 with chabazite (CHA) structure features pore sizes 0.38 X 0.38nm, through which only small hydrocarbon can diffuse. For example benzene is too large to go out the cage, which can explain in Fig 7 b the main product are ethylene and propylene, small amount of butanes and very little of linear alkanes. Fig6c the aluminosilicate zeolite ZSM-5 with the MFI structure whose pore size 0.55 X 0.51nm , a little larger 10MR zeolite compared with 8MR zeolite SAPO-34.And also from the Fig 7d we can see that the main product of ZSM-5 are methylbenzenes and light alkanes especially isobutane and isopentane and also olefins. Fig 7e the aluminosilicate zeolite Ferrierite with the FER structure pore sizes 0.54 X 0.42nm, which has similar acid strength with ZSM-5

and different structure. And from the Fig 7f we can see that the difference of structures result in different product distributions, the main product of FER are almost entirely olefins, especially butenes and pentenes.

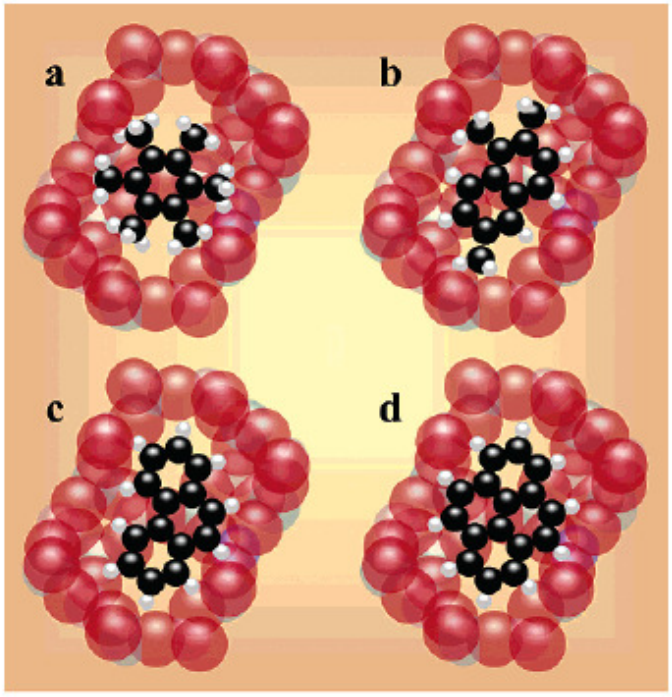

Fig.8 Molecular view of MTO catalyst deactivation shown for the specific case of HSAPO-34. (a) Hexamethylbenzene and other methylbenzenes are present in a few percent of cages in an active MTO catalyst. (b) With increasing time on stream, some of the methylbenzenes age into methylnaphthalenes. (c) Further aging to pheananthrene causes a loss of MTO activity in HSAPO-34. (d) The largest ring system to form in HSAPO-34 is pyrene[27, 28].

The fifth and final steps of MTO are catalyst deactivation. With time on stream, methylnaphthalenes (Figure 8b) are formed from methylbenzenes (Figure 8a)[27]. And then phenanthrene pyrene and the largest aromatic ring system will be accommodated in the catalyst' nanocages[28], until the polycyclic aromatics occupied the significant fraction of the cages which lead to mass transport of reactants and products reduce in the end. The used catalyst can be regenerated by calcined in air for few hours.

1.4 Objective of the study and precedents

Since the recent rise of oil prices and the need to reduce greenhouse emissions,

the transformation of methanol and other biomass-derived alcohols to hydrocarbons has became of renewed interest.

Alcohols can be converted to gasoline range hydrocarbons or short olefins depending mainly on the nature of the catalyst used. Among the short olefins, propylene has shown a growing demand in the past years mainly for the polypropylene industry. Catalyst based on zeolites ZSM-5 and the silicoaluminophosphate SAPO-34 are being industrially used for the conversion of methanol.

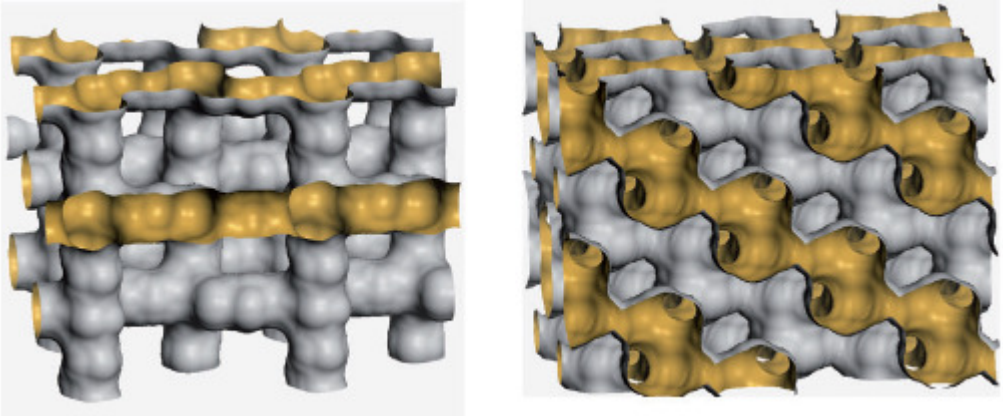

Fig. 9 Shape and connection of the internal surface to the two zeolites that are in industrial use: H-ZSM-5 (left) and H-SAPO-34 (right). Both materials have a three-dimensional channel structure, but the shape is very different. The surface in H-ZSM-5 is best described as interconnected tubes, while H-SAPO-34 has larger cavities with narrow connections[29].

The main differences in the performance of the 10MR zeolite ZSM-5 and the 8MR SAPO-34 are selectivity and deactivation by coke. ZSM-5 can be synthesized with low amount of framework aluminum in order to decrease the yield to aromatics and increase propylene; in addition, the MFI structure presents a tridimensional structure in which crossing channels do not create cages big enough to trap aromatic compounds that otherwise would act as coke precursors deactivating the catalyst. As a result, lifetime is reported to be higher than 500h. On the other hand, SAPO-34 of CHA structure defined by 8MR channels with cages in which aromatics are trapped, presents a faster deactivation increasing the number of regeneration cycles. However, the selectivity to olefins is higher for SAPO-34 than for ZSM-5 and it can be tuned to change the C_2/C_3 ratio[30].

In the recent years other different materials have shown interesting properties as catalyst for methanol to olefins but none have been used in a commercial scale. SSZ-13, the analogue zeolitic CHA structure has been studied [31, 32] but deactivates faster than SAPO-34. Other 8MR zeolites and SAPO's studied have been SAPO-17, ERI, LTA, UFI [33] and RUB-13[34]. All zeolitic structures showed higher deactivation rate than CHA, due to the higher size of the cavities.

While selectivity can be tuned to propylene when using SAPO-34 by changes in catalyst and process, extending lifetime as much as possible would greatly increase the profitability of the process. A great effort has been done in the case of ZSM-5, in which lifetime has been extended by increasing mesoporosity while preserving the micropore, that is designing hierarchical structures. It has been done by several ways: desilication, nanosheets of ZSM-5 or co-templating (carbon black and other organics). Some methods have been shown more efficient than others because it has been shown that when internal defects are developed, deactivation is enhanced. In summary it was shown that when diffusion of reactants and products is facilitated, coking is slowed and lifetime increased. A similar result was obtained when small or nanosized particles of ZSM-5 have been synthesized in which intraparticle mesoporosity is very high by itself [35].

When similar methods of developing mesoporosity have been translated to SAPO-34 and other 8MR zeolites, the expected increase in lifetime was not always attained. Sommer et al, could not improve lifetime of SSZ-13 by basic treatments. However, the addition of co-templates like amines or surfactants did obtain an increase in mesoporosity and lifetime for SSZ-13 (Wu SC-0.14 FEZA 2011) and SAPO-34 [36]. And recently, different methods of synthesis have reduced the particle size of SAPO-34 until nanometer scale, with a comparable improvement in lifetime. Dry gel synthesis methods have been studied by a lot of scientists [37, 38]. Also the uses of combinations of different SDA for the synthesis of SAPO-34 have been investigated with the objective to enhance lifetime. Lee et al [39] found that a combination of TEAOH and morpholine reduced the size of the crystals and then, lifetime increased. Wang [40] also studied the combination of TEA and TEAOH with

an improvement in lifetime, and very recently Alvaro-Muñoz et al. [41] compared different SDA and remarked the importance of high external surface, smaller crystal size and high acidity for the lifetime of SAPO-34.

Once it is clear the benefit of a higher external surface in the lifetime of SAPO-34 for the MTO reaction, it can be easily achieved by synthesis of nanosize SAPO-34 samples in which the contribution of the external to the total surface is very important. However, the stability of nanosized SAPO-34 could be a concern. Moreover, it is known that the structure of silicoaluminophosphates is affected by hydration because the Al-O-P bonds are easily hydrolizable [42], and in the case of sapo-34 its stability depends on the template used. In fact SAPO-34 synthesized with morpholine as SDA it is known to deteriorate irreversibly after long-term hydration [43, 44]. In order to increase the long-term stability of SAPO-34 based catalysts researchers from ExxonMobil found that the reversible treatment with NH3 increased the hydrothermal stability of SAPO-34 [44] and other post-synthesis treatments are claimed to protect or increase the stability by chemisorption with nitrogenated compounds as ammonia, amines or others ([45], [46], [47]). Besides, it was claimed that the treatment of activated SAPO-34 with steam also increases the hydrothermal stability [48].

In this work we have synthesized nanosized samples of SAPO-34 following the method of Yu et al [49] and have studied the activity, lifetime and selectivity in the reaction of methanol to olefins. In addition, we have studied the evolution of the stability for storage of nano sized SAPO-34 at room atmosphere. We have compared the catalytic performance and stability of nanoSAPO-34 with other sample of SAPO-34 synthesized by conventional hydrothermal methods using a mixture of morpholine and TEAOH as structure directing agents, which has been reported to give also small crystal size [39]. Finally, we have studied the influence of the steam treatment in the hydrothermal stability and lifetime of both samples.

2. Experimental

2.1 Synthesis of materials

Nano SAPO-34

SAPO-34 was synthesized by following the procedure reported by Lin et al [50]. by microwave heating in a program. The composition of the synthesis gel was 1.0 $Al(OPri)_3$: 2.0 H_3PO_4 : 2.0 TEAOH : 0.3 SiO_2 : 30 H_2O, $Al(OPri)_3$.Normally, isopropoxide $Al(OPri)_3$ was firstly mixed with TEAOH solution (35 wt%, Aldrich) and deionized water at room temperature until dissolved completely. Silica source [tetraethylorthosilicate (TEOS)] was then added and stirred for 2 h. Finally, phosphoric acid (85 wt% in water) was dispersed slowly into the above solution. The reaction mixture was further stirred for 1 h and then transferred into a Teflon autoclave. The crystallization was conducted in a microwave oven (Milestone ETHOS-D) with pre-programmed heating profiles at 180℃ for 1 h. The product was separated by high speed centrifugation, washed thoroughly with deionized water and ethanol, and then dried overnight at 50℃. The as-synthesized crystals were calcinated at 550℃ in air for 6 h to remove the template molecules. This sample will be called NanoSAPO-34.

Standard SAPO-34

For comparison purposes, other sample of SAPO-34 was synthesized following hydrothermal conventional method, with a mixture of morpholine and TEAOH 1:1 mol/mol as SDA with a gel composition of 1 Al_2O_3 : 1.06P_2O_5 : 1.08 SiO_2 : 2.09R : 66 H_2O. First distilled water mix with phosphoric acid and then psedoboehmite (Merck 85%) was added slowly with stirring into this solution and stir thoroughly for 7 hours, this called solution A. Fumed silica (Degussa Aerosil-200 99% SiO_2) and morpholine (Aldrich 99% C_4H_9O) mix thoroughly with water, this called solution B. Add B drop wise to A with stirring and stir thoroughly for 7 hours, and then move to 150 mL Teflon-lined autoclave 200℃ for 24 hours

Nano SAPO 1.0 $Al(OPri)_3$: 2.0 H_3PO_4 : 2.0TEAOH : 0.3 SiO_2 : 30 H_2O

Standard 1 Al_2O_3 : 1.06P_2O_5 : 1.08 SiO_2 : 2.09R : 66H_2O.

The ICP tests results were as below:

Nano Si/Al	0.54	Si 3.4 mmol/g
Standard Si/Al	0.3	Si 0.82mmol/g

2.2 Characterization

The samples were measured by X-ray powder diffraction (XRD) on a Panalytical CUBIX diffract meter with monochromatic CuKα1,2 radiation (λ=1.5406, 1.5444 Å; Kα2 / Kα1 intensity ratio=0.5)

The morphology and particle size were characterized by scanning electron microscope (SEM, JEOL JSM-6300). The samples were placed on a carbon film.

Elemental composition was determined by inductively coupled plasma atomic absorption spectroscopy (ICP-OES) using a Varian 715-ES.

Transmission electron microscopy requires that the fraction of the incident beam of electrons is transmitted through the sample, so that the thickness of samples must be thin enough to allow this. Scanning electron microscopy has a resolution of 5-15nm, while the transmission is 0.2-0.5nm.

Sample preparation consisted of dispersion the samples in a solvent (ethanol) using ultrasound. A drop of this dispersion was placed on grid coverage. The microscope used was a Philips EM400

The BET surfaces were measured by N2 adsorption and desorption at 77 k, pore volume and distribution of the pore volume in solids using various models. And the machine used for N2 adsorption and desorption was ASAP 2000 automatic equipment.

Low-temperature infrared spectroscopic (FTIR) experiments were performed in a Bio-Rad FTS-40A spectrometer using, respectively, a homemade stainless steel cell and a quartz cell fitted with KRS-5 windows, both connected to a vacuum dosing system. Before each experiment, the catalysts were pressed into self-supported

wafers (5–10 mg/cm2) degassed under vacuum (ca. 10−5 mbar) at 673 K and then cooled down to RT under vacuum. For low-temperature CO adsorption experiments, the samples were cooled to 77 K followed by CO dosing at increasing pressure (0.4–8.5 mbar) and recording the IR spectrum after each dosage. After CO dosing, the samples were evacuated and the spectra collected.

TPD experiments employed a Micromeritics 2900 apparatus. A calcined sample (100 mg) was activated by heating to 400ºC for 2 h in an oxygen flow and for 2 h in argon flow. Subsequently, the samples were cooled to 176ºC, and NH3 was adsorbed. The NH3 desorption was monitored with a quadrupole mass spectrometer (Balzers, Thermo Star GSD 300T) while the temperature of the sample was ramped at 10ºC min-1 in helium flow. Total ammonia adsorption was measured by repeated injection of calibrated amounts of ammonia at 176ºC until saturation. Ammonia desorption was recorded by means of the mass 15, because this band suffers less interference from the water desorbed by the sample.

2.3 Methanol to Olefin test

The catalyst was made to 0.2-0.4 mm particle size, and mix with 2 g quartz (Fluka), and then was put into a bed reactor. The methanol was bubbled with a nitrogen flow of 19 mL/min, the WHSV was about 7 h^{-1}. The catalyst was first activated by nitrogen flow of 80 mL/min for 1 h at 540℃, and then the temperature down to reaction condition 400℃. Each experiment was analyzed by an online gas chromatograph (VARIAN 450 GC, Pona and Al_2O_3 capillary columns, TCD and FID detectors). After reaction, the catalyst was regenerated at 540ºC in 80ml of air for 3h. and the reaction was done again.

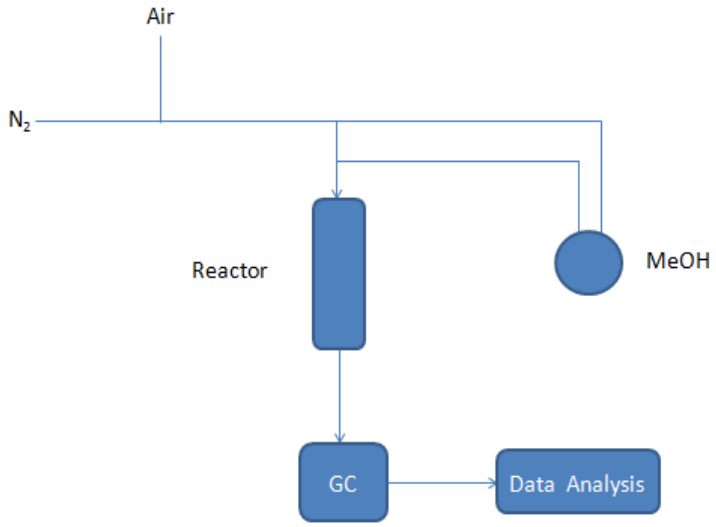

Fig 10 The scheme of methanol to olefin reaction system

3 Results and discussion

3.1 XRD and Microscopy

The XRD results of nano and standard SAPO-34 samples are shown in Figure 11 and 12 after exposure to air in room conditions for several days in which moisture of air is in contact with the samples. From the Fig. 11 (A) the samples of nano-SAPO-34 present as expected, a diffraction pattern with very low resolution similar to that reported by Lin et al [49], due to the small size of the crystals and there is no clear indication of any decrease in intensity after exposition at room conditions, even the samples were put in the lab for 40 days. To test the hydrothermal stability, we have treated the samples with 100% steam at 700 ºC for 5h. And the XRD result was shown in Fig. 11 (B). This time we can see the little changes in intensity for the steaming Nano SAPO-34, and main peaks were still the same with that calcined Nano one.

The standard SAPO-34 of large crystal size shows a diffraction pattern more intense and also there was no modification after several days of exposure to moisture from the Fig 12 (A). The standard steaming of SAPO-34 samples also reduced the intensity of the XRD peaks. From the point of view of XRD the structure of both

Nano and Standard SAPO-34 is not strong affected during neither the storage nor the steaming treatment. However, the broadening of the peaks in the diffraction pattern of nano SAPO-34 due to the small size of crystal does not allow to appreciate large changes in crystallinity.

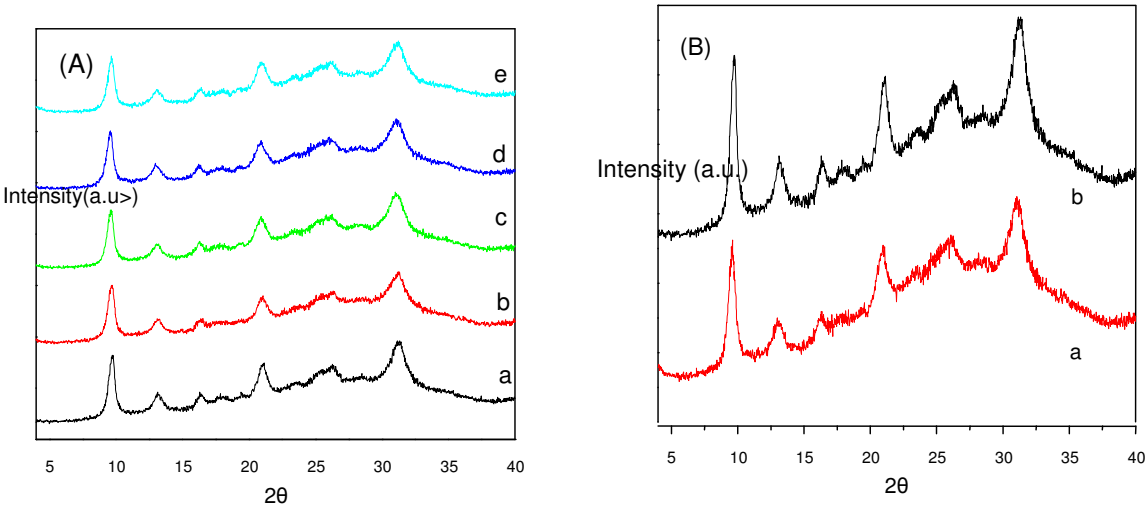

Fig.11 (A) XRD of nano SAPO-34 a) 1day b) 7days c) 14days d) 21days e) 42days of storage at room atmosphere after calcined

(B) a) Steamed Nano SAPO-34 b) nano SAPO-34

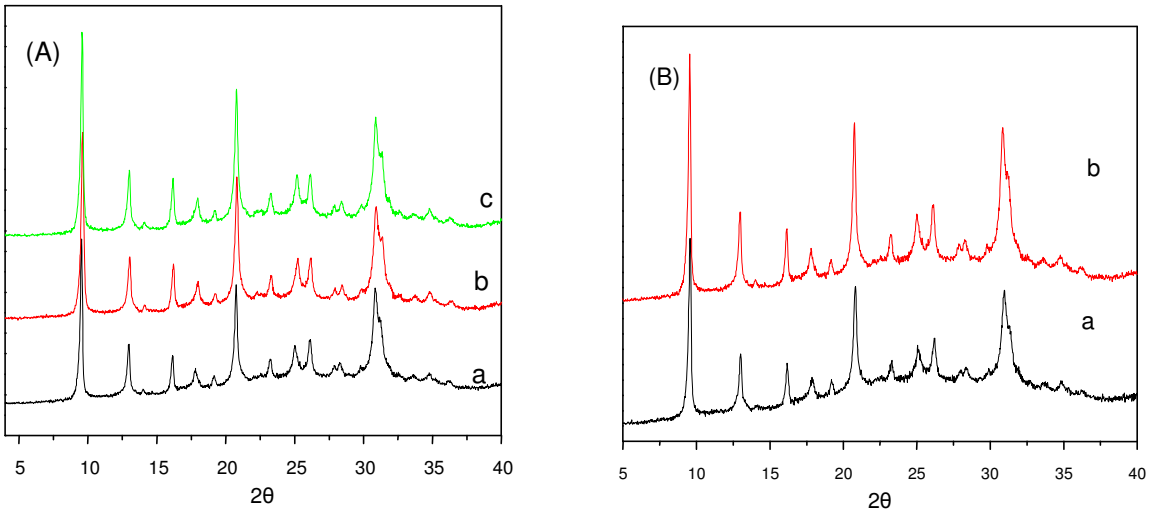

Fig.12 (A)XRD of standard SAPO-34 a) 1dayb) 21days c) 42 of storage at room atmosphere after calcined

; (B) a) steamed Standard SAPO-34 b) Standard SAPO-34

Fig.13 shows the SEM and TEM images of Nano SAPO-34 prepared by

microwave heating and the Standard SAPO-34. The sample Nano-SAPO-34 shows spherical aggregates of 150-300 nm formed by smaller crystals of around 20-50 nm, while standard SAPO-34 presents cubic crystals about 300-600 nm. The smaller dimensions of the crystals of Nano SAPO-34 agree with the broad XRD peaks showed in Figure 12, and the size of standard SAPO-34 is in agreement with the examples reported by Lee et al[39], in which SAPO-34 synthesized with the same mixture 1:1 of morpholine and TEAOH also presented crystal size in sub-micrometer range.

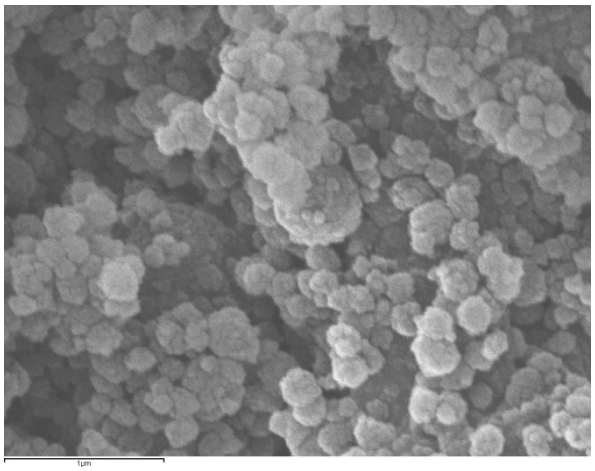

Fig.13 (A) SEM of Nano SAPO-34

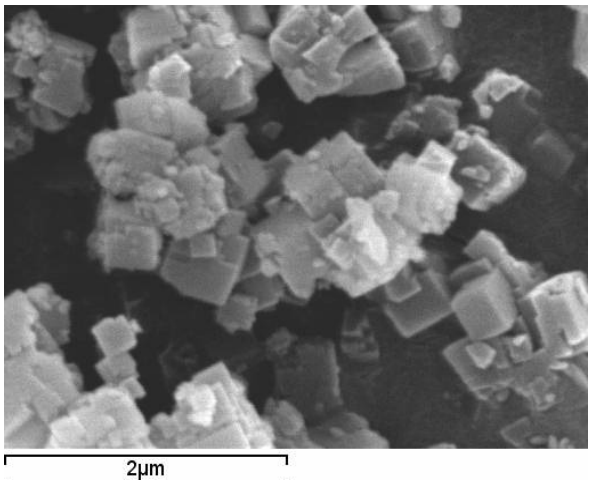

Fig.13 (B) SEM of Standard SAPO-34

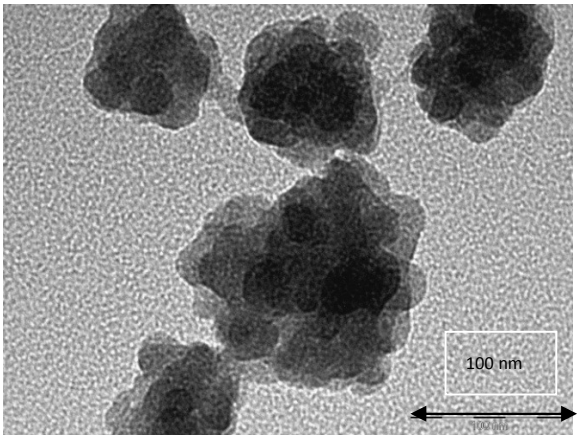

Fig.13 (C) TEM of Nano SAPO-34

3.2 N_2 Adsorption

Textural properties of samples are shown in Table 1. Nano SAPO-34 shows very high external surface area due to the small size of the crystals. After contact with ambient moisture for several days, the micropore volume steadily decreases while external surface area seems not to be affected, but after 28 days later the BET surface seemed to be changed from 613.2 to 560.5 m^2/g, and also the micropore volume reduce to 0.1815 cm^3/g. On the contrary, standard-SAPO34 presents an initial lower external surface area and BET, which does not seem to be affected after 2 months of moisture exposure, maybe the conclusion could be like that, in the room condition the BET surface of Standard SAPO-34were more stable than Nano one. And the reason maybe the Nano particle crystal samples would have some amorphous part with days increased which block the channels for N_2 adsorption and desorption.

Table 1 N_2 Adsorption of Nano SAPO-34

sample	BET (m^2/g)	t-plot Exter (m^2/g)	MPV (cm^3/g)	Meso Volu (cm^3/g)
Nano SAPO-1day	646.1	230.5	0.2032	0.2087
Nano SAPO-7days	639.3	226.3	0.2019	0.2058
Nano SAPO-21days	616.3	223.6	0.1920	0.2004
Nano SAPO-28days	613.2	223.9	0.1904	0.2011
Nano SAPO-42days	560.5	182.0	0.1815	0.3273
Nano SAPO-107day	535.5	223.3	0.1527	0.1979
Steaming Nano SAPO 1 days	490.3	162.6	0.1604	0.1816
Steaming Nano SAPO 50 days	488.1	160.2	0.1606	0.1852
Steaming Nano SAPO 65 days	490.9	162.8	0.1607	0.1932

After steaming at 700 ºC for 5 hours, both of Nano SAPO-34 and standard one presented a reduction in micropore volume and external surface, but the steaming Nano one's values are yet higher than those of standard SAPO-34, and values are more stable compared the Nano one. Even after 65 days of storage at room conditions, the value were almost the same. The external surface of standard SAPO-34 was not affected by steaming and micropore volume is slightly reduced.

Table 2 N_2 Adsorption of Standard SAPO-34

Sample	BET (m^2/g)	t-plot Exter (m^2/g)	MPV (cm^3/g)	Meso Volu (cm^3/g)
Standard SAPO 5 days	450.0	63.03	0.1903	0.1105
Standard SAPO 29 days	462.6	62.48	0.1966	0.1147
Standard SAPO 44days	462.9	64.78	0.1957	0.1114
Steaming Standard SAPO-2days	432.0	67.72	0.1791	0.1099
Steaming Standard SAPO-54days	404.1	60.43	0.1695	0.1135
Steaming Standard SAPO-62days	429.8	67.50	0.1782	0.1135

The corresponding spectra are given in Fig.14. Calcined nano SAPO-34 shows an intense peak at 36 ppm followed by other signals at -11 and -14 ppm, that corresponds to tetracoordinated aluminum in local structures of $Al(PO)_4$, and octa and pent coordinated aluminum coordinated, respectively [42]. After 7 days of storage, the signal at 14 ppm continuously increased indicating hydration of $Al(PO)_4$ species [42, 51], while the signal of tetracoordinate aluminum is shifted to -41 ppm. The shifting of the tetrahedral signal could be attributed to a distortion of the framework due to the hydration of the structure [52]. The standard SAPO-34 sample shows the same signals, with lower intensity of octahedral aluminum possibly due to a lower effect of hydration that is accompanied with a lower shifting of the tetrahedral signal at 36 ppm. When both samples are submitted to steaming at 700 ºC, the spectrum similar with signals at 40, -11 and -14, but the intensity of octahedral

aluminum is lower for nanoSAPO-34.

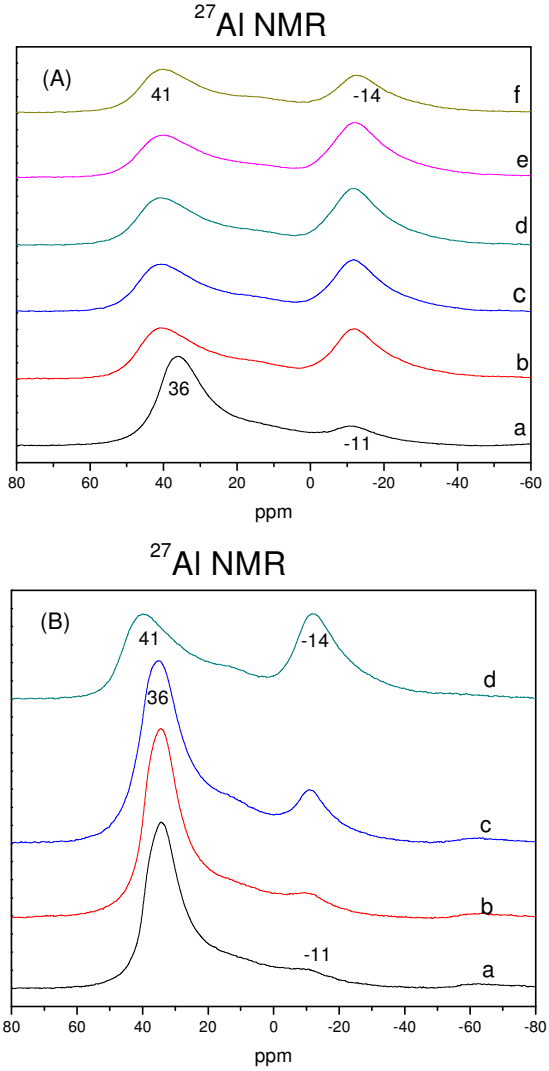

Fig.14 (A) 27Al NMR of nano SAPO-34 a) 1dayb) 7days c) 14days d) 21days e) 42days f) steamed nano SAPO-34 (B) standard SAPO-34 a) 21 day b) 32 days c) 40 days d) steamed standard SAPO-34

3.3.2 ^{28}Si NMR

The ^{28}Si NMR spectrum of nano and standard SAPO-34 is shown in Figure 15. This technique is useful to study the mechanism of silicon incorporation in the framework of $AlPO_4$. In silicialuminophosphates, silicon is incorporated following two different mechanisms, SM2 in which a single Si substitutes a single P atom, or SM3 in which two Si atoms substitutes two neighbors' Al and P atoms [53, 54]. Nano SAPO-34 shows a broad signal formed by components at -89, -95, -100, -105 and -110 ppm, that corresponds to $Si(OAl)_4$, $Si(OAl)_3$, $Si(OAl)_2$, $Si(OAl)_1$ and Si(0Al)

respectively [52, 54-56]. The incorporation of silicon through SM2 generates $Si(OAl)_4$ groups while mechanism SM3 generates the others. Thus, there is an important participation of the SM3 mechanism substitution together with SM2 for nanoSAPO-34. It has been reported that the contribution of mechanism SM3 in SAPO-34 depends on the proportion of silicon was high in the gel composition [41, 57, 58].However, conventional hydrothermal synthesis performed with TEAOH as SDA and higher amount of silicon has been reported to produce SAPO-34 samples in which substitution mechanism is preferentially SM2. Thus, synthesis performed by microwave heating could induce more incorporation of silicon through mechanism SM3, in which two silicon atoms replaces an Al and P pair.

After 7 days of hydration, the signal at -95 ppm corresponding to Si(OAl)3 decreases and a broad small band around -78 to -85 appears. This broad band has been assigned to Q1, Q2 and Q3 entities [43], $Si(OAl)_4$ disordered [42] or Si located at the edge of a Si domain [59]. In any case, this band has been reported to be enhanced by cross-polarization [43, 59], that suggests that are defect sites created by hydration and hydrolysis. Therefore, it appears that $Si(OAl)_3$ species are first affected by hydrolysis creating groups $Si(OAl)_{(3-x)}(SiOH)_x$. At increasing time of hydration the band corresponding to defects increases at expenses of the bands -89 to -99 ppm. It is important to note that silicon species incorporated by SM3 mechanism are first affected by hydrolysis, because their associated Brönsted acid sites are stronger than those generated by single Si incorporation (SM2). In fact, recently Katada et al. [60] studied different SAPO-34 and determined that samples with less isolated Si presented weaker Brönsted acidity and attributed the stronger acidity to the presence of distorted structure including SiO_2 islands or defects. Other authors, [55, 61] in the line of the contribution of Barthomeuf [62] assign the higher acidity to the presence of silicon islands in which acid sites are generated in its borders. Consequently, in our case for nanoSAPO-34 the silicon species first affected by hydrolysis are those that generated stronger acid sites and then, the overall acidity should be decreased by hydrolysis and its strength shifted to milder acidities.

The standard SAPO-34 sample shows sharper signals of ^{28}Si NMR at the same

positions that Nano SAPO-34, with higher intensity of the signals at -105 and -110 corresponding to $Si(OAl)_1$ and Si(0Al) due to its higher silicon content. However, the changes after several days of hydration are slower. After 32 days of hydration the signal at -95 ppm corresponding to $Si(OAl)_3$ starts to decrease, and only after 40 days, the signal of defects from -78 to -85 ppm are visible. Again, the standard SAPO-34 is shown less sensitive to hydrolysis than nanoSAPO-34.

After steaming at 700 ºC, some slight differences appear comparing with the hydrated samples. In the case of steamed-nanoSAPO-34, comparing with the sample hydrated 43 days, the steaming treatment caused an increase in the intensity of the signals at -100 to -110 corresponding to Si in SiO_2 islands while the signals corresponding to single silicon Si4Si and Si in the border of SiO_2 islands Si3Al1Si have decreased. In the case of the standard SAPO-34 the effect of steaming is a small broadening of the signal, and the profile is very similar to that of the sample hydrated for 40 days. It is important to notice that when steaming nano SAPO-34, the signals at Si4Al and Si3Al1Si decreased with no proportional increase of defects. It suggests that with the presence of steam this two silicon species migrate to silicon islands without the appearance of defects.

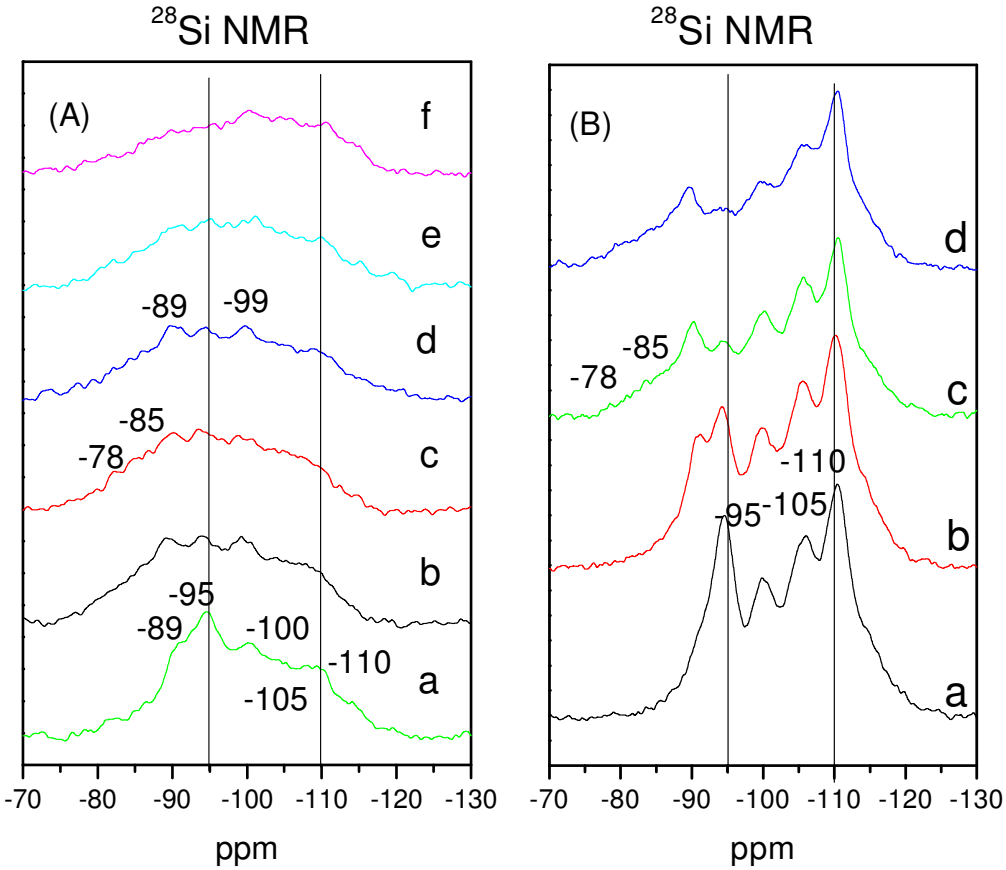

Fig.15 (A) ^{28}Si NMR of nano SAPO-34 a) 1day b) 7days c) 14days d) 21days e) 42days f) steamed nano SAPO-34 (B) standard SAPO-34 a) 21 day b) 32 days c) 40 days d) steamed standard SAPO-34

3.3.3 ^{31}P NMR

The ^{31}P NMR spectra (Fig 16) for fresh nanoSAPO-34 shows an asymmetrical signal at -30 ppm corresponding to tetrahedral $P(OAl)_4$. After 7 days of hydration other signal at -16 ppm appeared corresponding to P atoms coordinated with water molecules in form of species $P(OAl)_x(H_2O)_y$ [42, 63, 64]. The relative intensity of the signal at -16ppm increased continuously even up to 42 days of hydration and correlates well with the increase in the octahedral signal of Al NMR at -12 ppm which was assigned to the hydration of the $Al(PO)_4$ species. In the case of the standard SAPO-34 sample, the only signal that appears is the corresponding to tetrahedral phosphorus at -30 ppm up to 40 days of hydration. After steaming, both samples present signals at -30 and -16 ppm, the latter caused by hydration with the steam being more intense in the case of steamed-nanosapo-34.

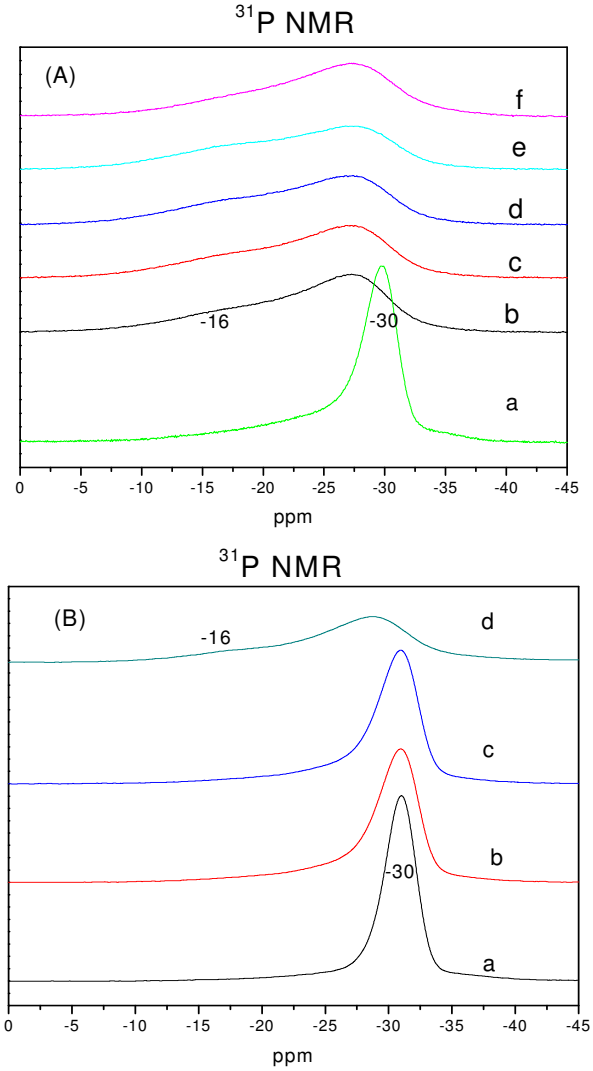

Fig.16 (A) ^{31}P NMR of Nano SAPO-34 a) 1day b) 7days c) 14days d) 21days e) 42days f) steamed Nano SAPO-34 (B) standard SAPO-34 a) 21 day b) 32 days c) 40 days d) steamed Standard SAPO-34

3.4 FTIR and CO Adsorption

The FTIR spectrum of nanoSAPO-34 in the hydroxyl region is shown in Fig. 17-20. The sample nanoSAPO-34 shows characteristic signals at 3600 and 3630 cm^{-1} corresponding to low and high-frequency Brönsted OH groups, 3745 and 3678 cm-1 corresponding to external Si-OH and P-OH groups respectively, and other small signals at 3796 and 3770 cm^{-1} referred in the literature as OH groups linked to tetrahedral Al [65, 66] . The relatively high intensity of these latter two bands must be assigned to the high external surface of the sample. In addition, there is a broad band centered around 3400-3500 cm^{-1} which should correspond to Si-OH and P-OH

groups interacting through H-bonds, as reported for high silica CHA zeolites [67] and mesoporous AlPO [68]. After days of hydration this broad band increases in intensity indicating that defects are being developed. In addition, the band at 3678 cm^{-1} corresponding to P-OH groups also increases due to the irreversible hydrolysis of the Al-O-P bonds.

The adsorption of CO at low temperatures has been used to characterize the strength of the acid sites of SAPO-34. In the case of the sample of nanoSAPO-34, the bands corresponding to HF and LF Brönsted acid sites are shifted upon progressive adsorption and interaction with CO to a broad band around 3200-3500 cm^{-1} and are in agreement with that reported in the literature [55, 69]. In addition, two other bands in the CO-stretching area appear at 2171 and 2140 cm^{-1}, corresponding to CO interacting with Brönsted acid sites and physisorbed condensed CO respectively [69]. The broad band around 3200-3500 cm^{-1} is composed of a main signal at 3364 cm^{-1} and a shoulder at 3474 cm^{-1}. These signals have been assigned to CO interacting with HF and LF hydroxyls and, in agreement with the contribution of Martins et al [55], other overlapped signal appear at 3280 cm^{-1} if a deconvolution of the broad band is performed. Due to its larger shift, this overlapped band at 3280 cm^{-1} has been assigned to CO interacting with acid sites corresponding to Si in the borders of the silicon islands, with an acidity of higher strength. As shown above in the analysis of Si-NMR spectra, after days of hydration of nanoSAPO-34 it was also expected to see a decrease of those sites of higher strength if they are related to Si(3Si1Al). However, the fitting process for deconvolution of the overlapped bands showed a contribution of around 10% of the overall area of the broad band, being almost impossible to distinguish if there is a decrease in these sites due to hydrolysis and transformation in defects. In addition, the signal at 2171cm^{-1} due to CO adsorption on acid site after the first phase of CO.

The FTIR of nanoSAPO-34 steamed sample is very similar to the parent sample, with a decrease in the intensity of the broad band 3200-3500 cm^{-1} corresponding to Si-OH and P-OH groups interacting through H-bonds.

In summary, from the analysis of FTIR of adsorbed CO, it has not been possible

to see difference in acid strength of nano SAPO-34 samples at different time of storage. Possible, CO is too basic for measuring small differences in acid strength or after several pulses of CO the average of the signal does not show changes in wave number that could be an indication of different acid strength.

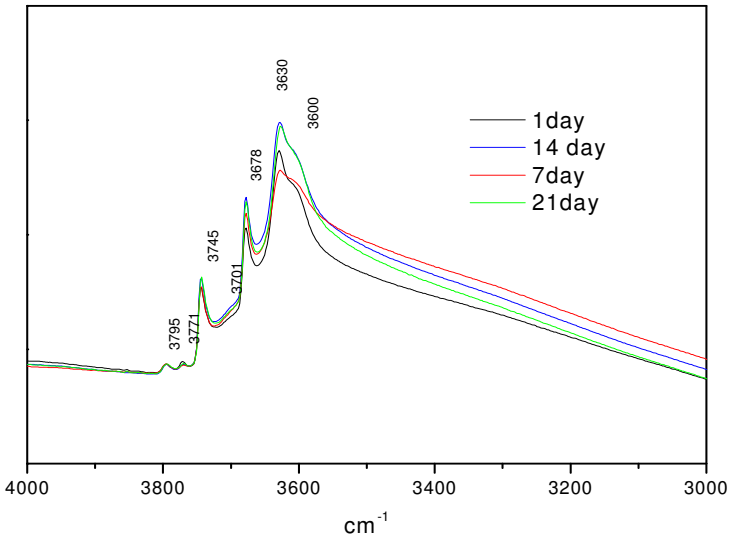

Figure 17. FTIR in the OH range of nanoSAPO-34 after storage at room environment.

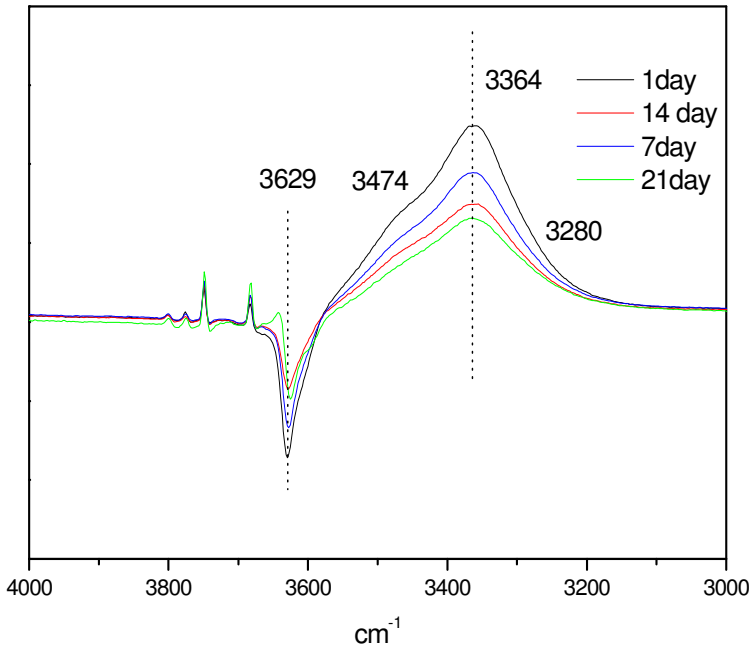

Fig.18. FTIR in the OH stretching range of fresh nano SAPO-34 after sequential pulses of CO adsorption. Spectra substracted from the original free of CO.

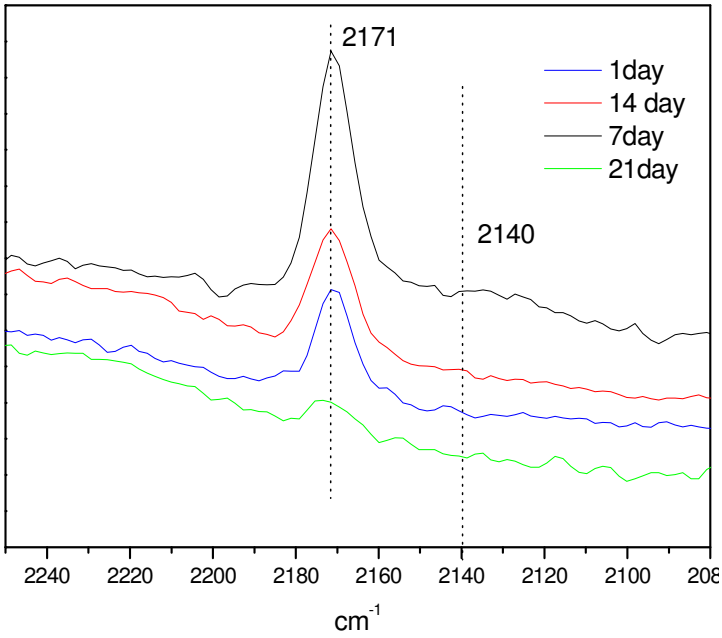

Fig.19. FTIR on the CO stretching after the initial CO adsorption on nanoSAPO-34 after storage at room environment for 1, 7, 14 and 21 days.

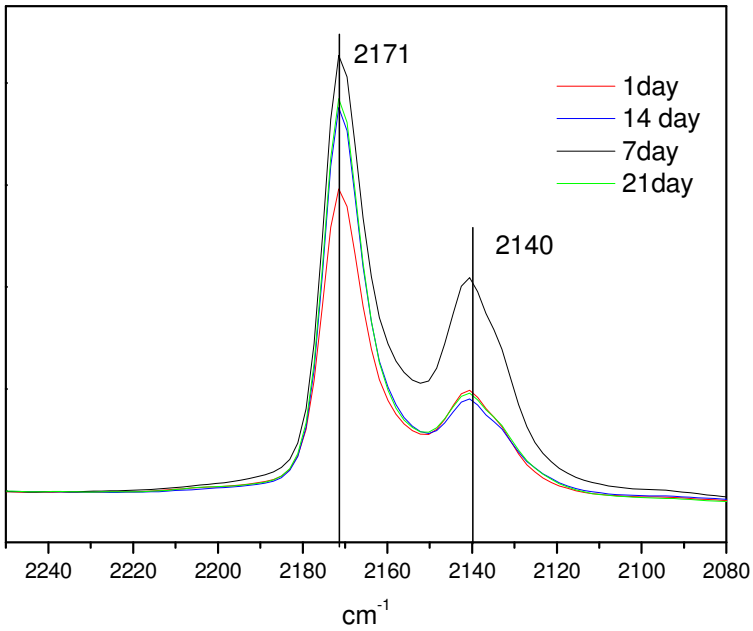

Fig. 20. FTIR on the CO stretching after several pulses of CO adsorption on nanoSAPO-34 after storage at room environment for 1, 7, 14 and 21 days.

Table 3 NH_3 Temperature program desorption

Days	Nano SAPO(mmolNH3 g-1 zeolite)	days	standard(mmolNH_3 g-1 zeolite)	steaming Nano(mmolNH_3 g-1 zeolite)	steaming standard(mmolNH_3 g-1 zeolite)
1	1.02907991	28	0.971424	0.530717411	0.733139
3	1.02814732	40	0.951022		
30	0.8602308				
43	0.71852054				
60	0.89214866				

3.5 Methanol to hydrocarbons activity

The activity of nano and standard SAPO-34 is shown in Figures 21-22 at WHSV=7h-1. It is important to note the higher lifetime of nanoSAPO-34. In addition, in the case of nanoSAPO-34, lifetime changes with the time of storage. First, it increases until maximum life after 14 days of storage and then decreases continuously. Standard SAPO-34 showed always a lower lifetime than that of nanoSAPO-34, and seems to stabilize after 42 days of storage

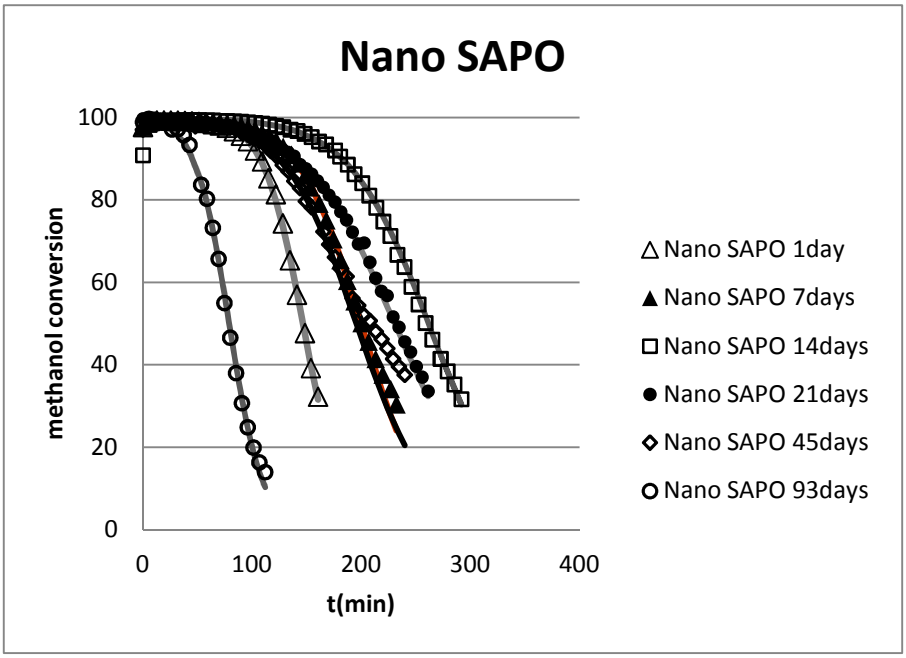

Fig.21 MTO reactions on different nano SAPO-34 after calcinations, have been exposed to room atmosphere froe 1up to 93 days.

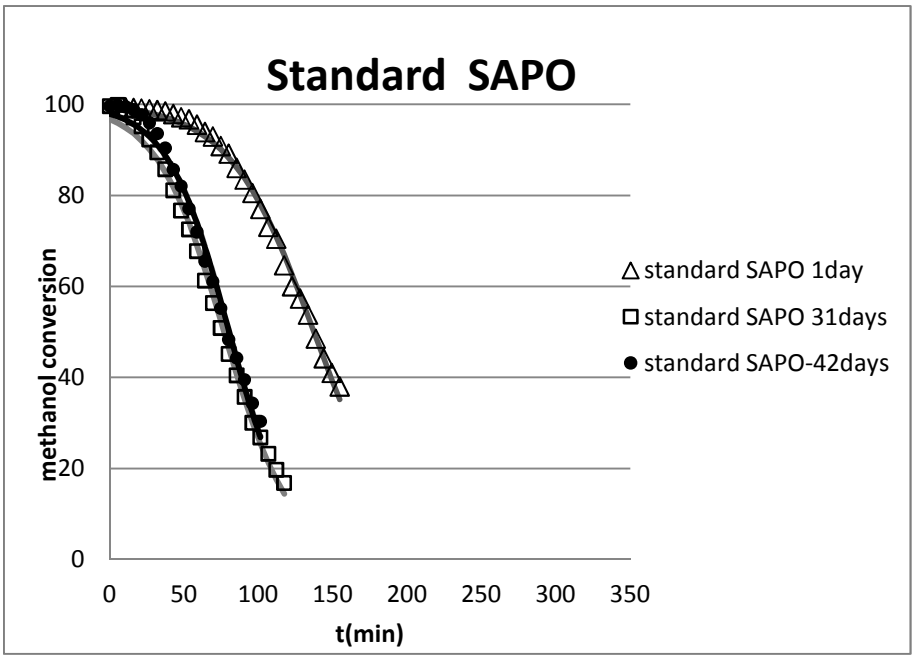

Fig.22 MTO reactions on different standard SAPO-34 after calcinations, have been exposed to room atmosphere from 1 up to 42 days.

Kinetics

In order to rationalize the different behavior of activity for the samples of SAPO-34, we have performed a kinetic analysis following the model proposed for Janssens[70, 71] for modeling the deactivation of ZSM-5 in the conversion of methanol to gasoline. Jannsens proposes that conversion of methanol to hydrocarbons on zeolites can be modeled just by using two parameters, the rate constant and the deactivation coefficient, assuming a first order of reaction and a deactivation rate proportional to the conversion. Also by following this methodology, half lifetime and charge capacity of methanol can easily be estimated.

The model proposed by Janssens considers deactivation as an effective decrease of contact time, and agrees with a "non selective deactivation" of the reaction, in which the successive steps from reactants to products are affected by deactivation at the same rate and can be modelized by a single parameter. It has been shown true for the oligomerization of olefins and also the reaction of methanol to gasoline in ZSM-5[72, 73]. However, the reaction of methanol to olefins on SAPO-34 was shown as "selective deactivation" by Chen et al [74, 75]. In our case, the fitting of the

conversion of methanol + dimethylether lumped for both SAPO-34 is surprisingly as good as shown in the literature in the case of ZSM-5, suggesting that also in this case a "single event kinetics model" can be used as in the case of SAPO-34.

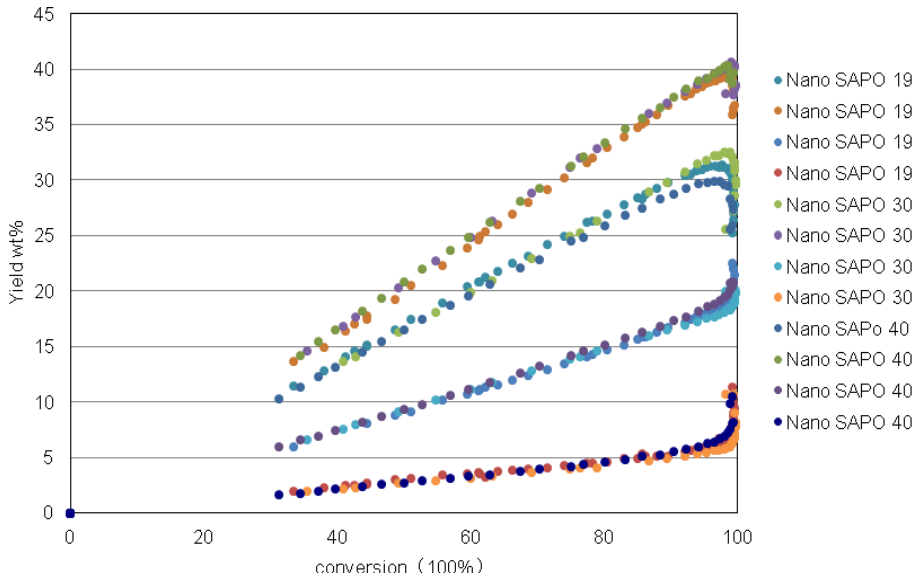

Fig. 22 Yields of C_2, C_3, C_4 and C_5+ in MeOH on nanosapo-34 (21 days aged) at different spatial times (7, 11, 15 h-1) at 400 ºC

In addition, the selectivity at three different spatial times were compared in Figure 20 and it was shown that basically selectivity is very similar at constant conversion and not depends on spatial time. So, also in SAPO-34 as in the case of ZSM-5, deactivation can be considered as a decrease of contact time that at the end is the same as a decrease in the amount of active catalyst during the time of the reaction.

Then, by fitting the following model (X: conversion, tau: spatial time gcat/mol h, a deactivation constant, K kinetic rate constant), parameters found are shown in table 4.

$$\frac{dX}{dt} = k(1 - X)$$

$$\frac{d\tau}{dt} = -aX$$

$$X = \frac{(\exp(k\tau_0) - 1)\exp(-kat)}{1 + (\exp(k\tau_0) - 1)\exp(-kat)}$$

Table.4 K and a value of all the samples

Sample: Nano SAPO-34

days	k	a
1	45.14	0.001235

7	38.92	0.0009065
14	39.98	0.0006918
28	30.87	0.0007847
45	33.15	0.0009251
93	28.63	0.002291

Sample: Standard SAPO-34

days	k	a
1	26.77	0.001317
32	18.87	0.002332
41	21.36	0.002241

It can be seen that the initial kinetic rate constant is much higher for nanoSAPO-34 than for the standard sample. It agrees with the smaller size of the crystals of nanoSAPO-34, since methanol reaction on eight member ring zeolites is diffusion controlled, higher external surface will greatly increase initial activity. And taking into account that both samples presented similar acidity measured by ammonia TPD, the kinetic rate constant obtained must be directly related to the number of accessible sites close to the surface of the catalyst. Indeed, after exposure to room atmosphere the kinetic rate constant steadily decreases in both nano and standard SAPO-34. The initial deactivation constant is similar for both catalysts. However its behavior after exposure to room atmosphere is different. In the case of nanosapo-34, the deactivation constant strongly decreases up to 14 days and then increases, while for standard SAPO-34 it continuously increases. The long-term increase in the deactivation constant could be due to the presence of defects created by the irreversible hydrolysis of the structure, as shown above by FTIR and NMR that could accelerate deactivation by adsorption of coke precursors. In fact, a higher deactivation and shorter lifetime was reported in the case of zeolite ZSM-5, in which the creation of internal silanol nests by carbon templating induced higher deactivation in the MTH reaction [76, 77]. On the other hand, the short-term decrease in the deactivation constant until the 14th day of exposure for nanoSAPO-34 could be attributed to the hydrolysis of the Si-O-Al groups at the border of the silicon islands shown before by NMR. These acid sites are believed to present acidity close

to those of zeolites and then, and then, will promote coking faster than single silicon sites in SAPO-34. Their disappearance by hydrolysis will enhance lifetime. Therefore, by selective hydrolysis of Si-O-Al bonds corresponding to strongest acid sites, the remaining acidity resulted in a catalyst with lower deactivation and longer lifetime.

Selectivity and thermodynamic equilibrium of olefins

When wt% yields and selectivity to olefins are plotted vs. conversion (Figure 23, 24), in general, selectivity is constant when conversion is not complete and changes continuously in case of full conversion. As a consequence, the C_2/C_3 ratio tends to increase with time on stream (Figure 26). It was already described by many authors. In fact, Chen et al. [78] showed that ethylene selectivity increased with increasing coke and proposed that coke has an effect of effective reduction of void volume of the cavities modifying the transition-shape selectivity through the formation of smaller molecules. On the other hand Dahl [79] and Barger [30] proposed that is product shape selectivity which controls product distribution and that higher ethylene selectivity is due to a faster diffusion of the shorter ethylene vs. the longer propene through 8MR windows. The latter proposition was supported by Hereijgers et al. [80] which by means of isotopic switch experiments with C13-marked methanol, presented hexamethylbenzene as the most active intermediate for the MTO reaction, even for the strong deactivated catalyst, that is independent of the amount of coke formed. However, if an easier diffusion of ethene were the main factor affecting the ratio C_2/C_3 with time on stream, it should be greatly affected by the size of the crystal of SAPO-34 by inducing higher C_2/C_3 values in case of larger crystals. When looking into the C_2/C_3 ratio of nano and standard SAPO-34, just the trend is the opposite. C_2/C_3 is higher for nanoSAPO-34 and increases with TOS, when as the samples are aged at room conditions, the overall ratio decreases. This effect must be related more in terms of acid strength than on diffusion. In fact, Song et al. [81] reported that selectivity of ethylene was favoured by methylbenzenes trapped in the cages with lower number methyl groups, while propylene is favoured

when the number is higher of methyl groups, and Arstad et al. [82] showed that the formation of ethylene from either hexa or tetramethylbnezene reaction center is energetically less favoured than propylene. So, it can be deduced that stronger acidities should induce higher C_2/C_3 ratios. In the case of fresh nanoSAPO-34, the presence of acid sites corresponding to Si in the border of silicon islands, could present higher strength and be the reason of the higher C_2/C_3 ratio, and when the number of these sites is reduced by hydrolysis at room atmosphere, the C_2/C_3 ratio drops sensibly.

On the other hand, the variation of the C_2/C_3 ratio with Time on Stream is restricted to the analysis in which conversion is close to 100% and it seems logical to think that thermodymamic equilibrium of olefins should occur and have a strong effect on selectivity.

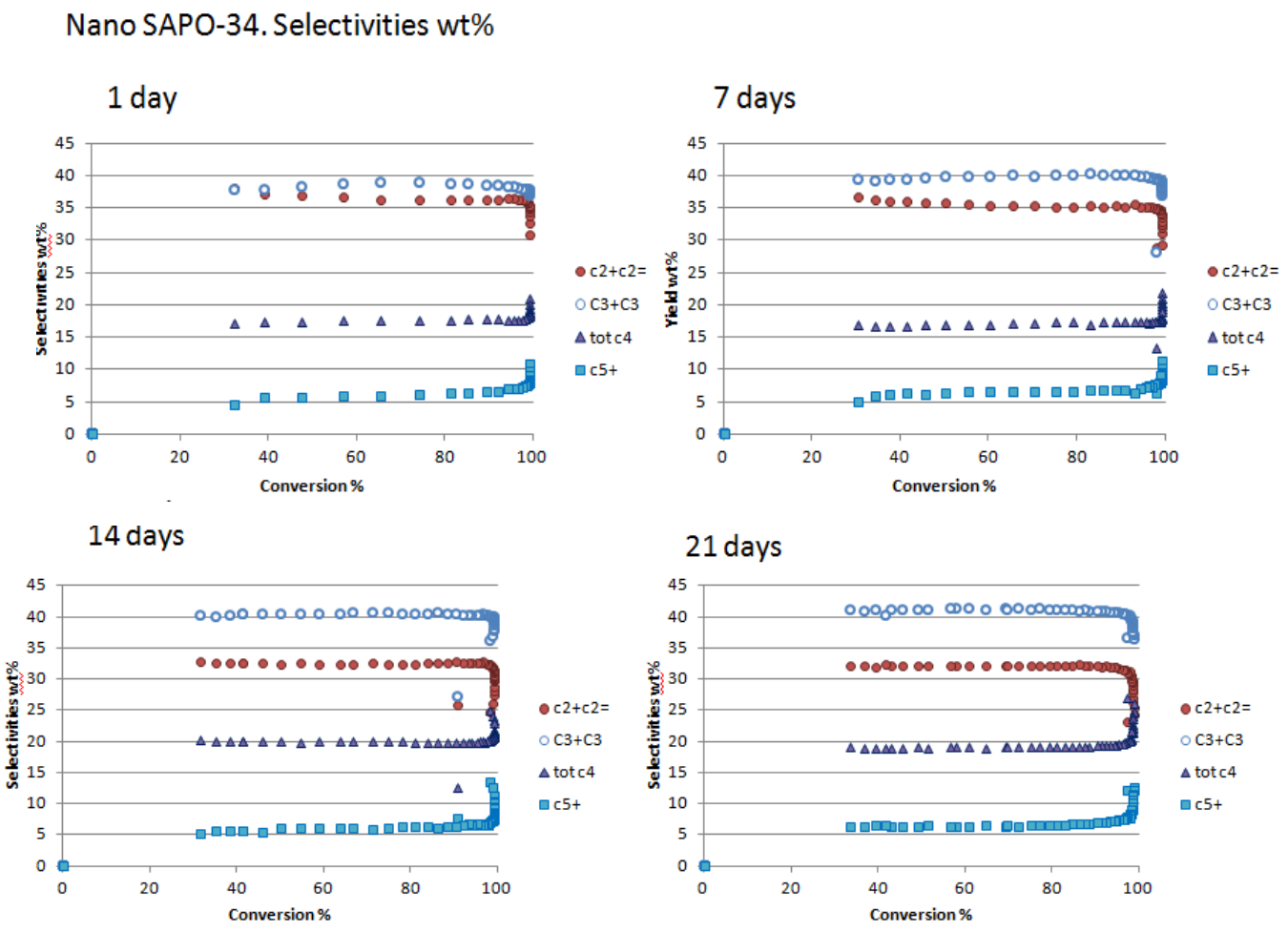

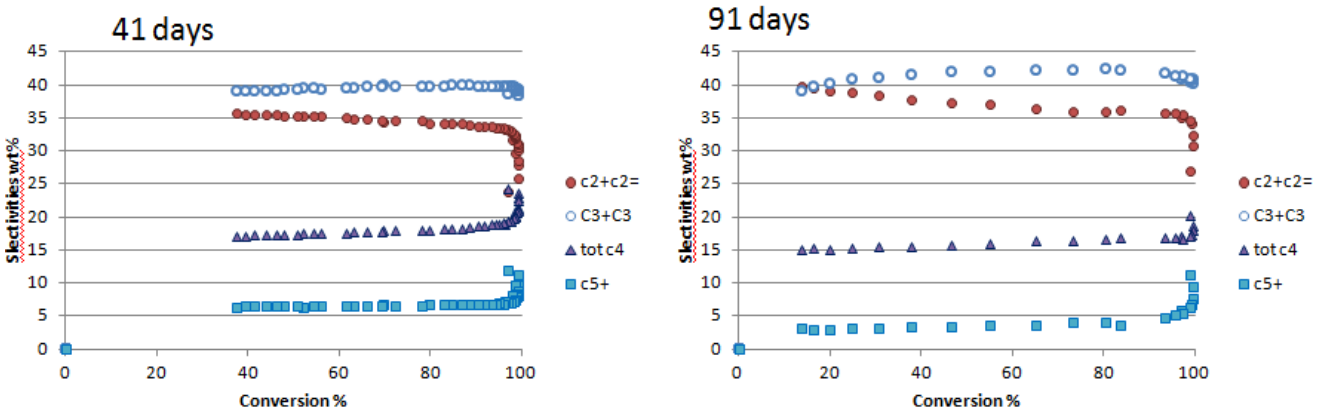

Fig 24 the selectivity of Nano SAPO-34 in different days

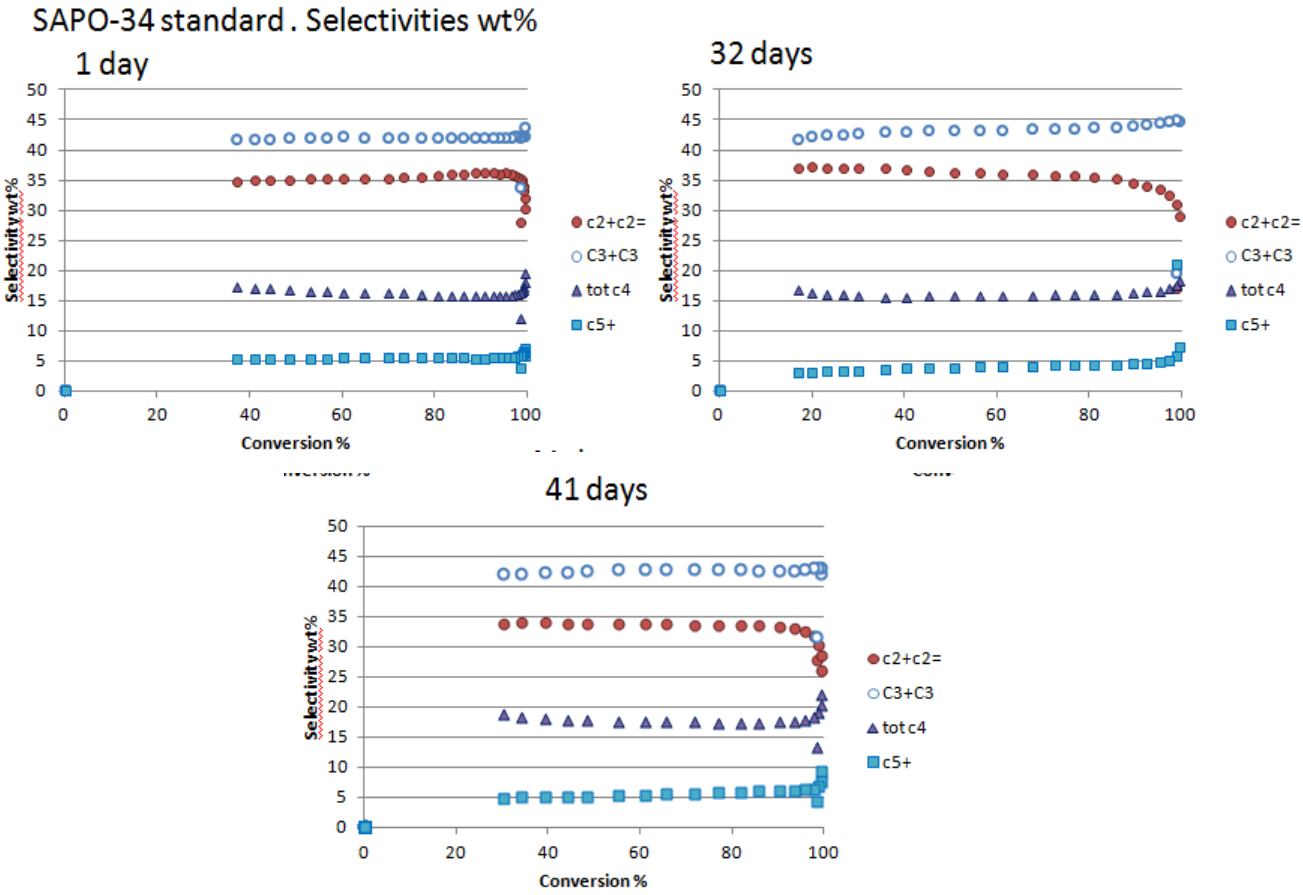

Fig 25 the selectivity of standard SAPO-34 in different days

In figure 24 and table 5, initial and steady-state selectivity are compared with thermodynamic values calculated including or not branched C_4 and C_5 olefins. It is important to notice the branched olefins obtained in the case of nano-SAPO-34 that must be attributed to the presence of higher amount of external surface area. In fact,

including branched olefins in the thermodynamic calculations leads to a different distribution of equilibrium, with lower amounts of C_2-C_3 olefins. In fact, the initial distribution of olefin in both SAPO-34 correlates with the different equilibrium distribution with the exception of ethylene, that is not surprising taking into account that in the transformation of different olefins, ethylene is very difficult to activate or protonate comparing with longer olefins. A similar result was obtained by Zhou et al [71] showing that the rate of conversion of ethylene on sapo-34 is much lower than propene and butane. In summary, at the start of the reaction, after the induction period, the olefins formed at the top of the bed are transformed in the fresh catalyst towards the equilibrium distribution, and in the case of nanosapo-34 with higher external surface, olefins can isomerize and branched C_4 and C_5 appear as products. As the deactivation front moves from the catalyst bed to the bottom, less fresh catalyst remains until breakthrough of conversion below 100 wt%, from where the selectivity reaches a steady-state, less affected by interconversion of olefins and approaching the original selectivity of the hydrocarbon pool. Therefore, while conversion during MTO reaction on SAPO-34 is close to 100%, that is the working parameter for the industrial unit, the selectivity to olefins is strongly affected by thermodynamical distribution. In addition, the differences in C2/C3 ratio after exposition to moisture, and also the comparison with the values obtained with the larger-sized Standard sapo-34 do not correlate with an easier diffusion of ethene vs. propene. Moreover, this result is more in agreement with "transition shape selectivity effect" in which higher amount distribution of products is affected by different acid properties of the catalyst and not to a "product shape selectivity" in which coking reduces the size of the cages and hinders diffusion of products.

Table.5. Initial and steady-state distribution of olefins in the conversion of Methanol to Olefins at 400ºC, WHSV 7h-1 on standard SAPO-34(1day) and nanoSAPO-34(14days). Thermodynamic equilibrium at P=0.04bar

Thermodynamic equilibrium		Standard SAPO-34		Nano SAPO-34	
Linear olefins	Linear+Branched olefins	Initial olefin distribution	Steady-state	Initial olefin distribution	Steady-state

Ethene	17.8	15	30.3	35	24.5	30.5
Propene	47.8	38.3	43.7	42	35.5	36.6
Butenes	28.2	26.8	19.7	15	24.6	20.8
Pentenes	6.2	19.9	7.3	5	13.4	10.6

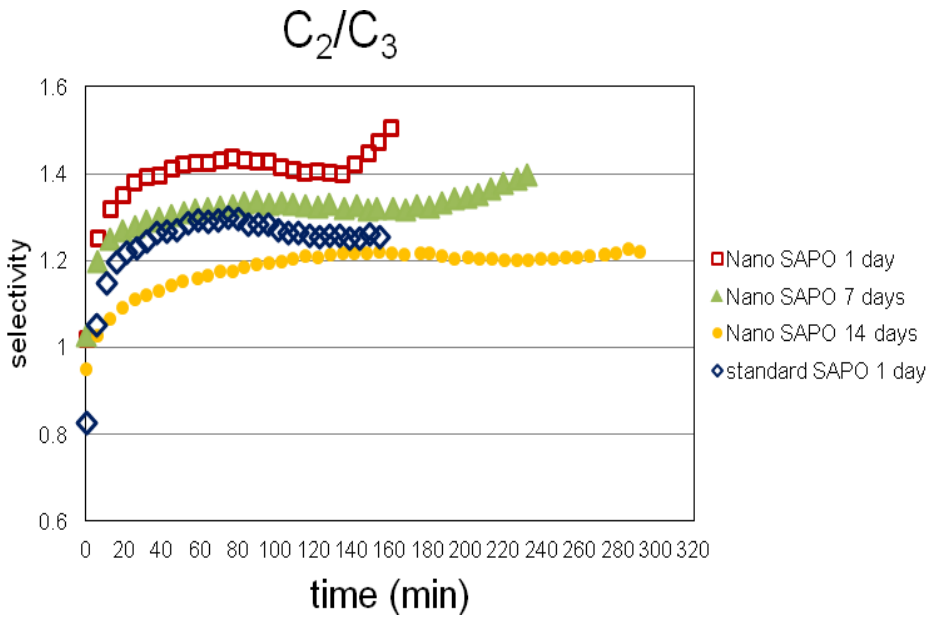

Fig 26. C2/C3 ratio in different days for nano and standard SAPO-34

3.6 Stabilization of nanoSAPO-34 by hydrothermal treatment

The activity of nanoSAPO-34 measured in terms of lifetime or charge capacity has been shown higher than standard SAPO-34 due to its smaller crystal size. However, its stability is lower after exposure to moisture at room conditions. In this part we will show how its activity can be stabilized by steaming at different temperatures.

Steaming of samples was done at 400, 500 600 and 700 ºC for 5 h and were tested in the MTO reaction at the same condition than before. From Fig.27-30 it can be seen that when Nano SAPOs were treated with steam, the activity in MTO was still better than that of standard SAPO-34, especially the sample steamed at 700ºC. If kinetic rate and deactivation parameter are compared for the steamed samples (Table 6), steaming causes a decrease in kinetic rate constant (K). It agrees with an effective

reduction of acidity of the samples with steaming, and an increase in an amorphous phase. The deactivation parameter (a) presents values similar to those of the fresh nano SAPO-34. It is important to notice that the sample steamed at 700ºC is stable after more than 60 days of exposure to moisture. At lower temperate of steaming, kinetic rates are higher with similar values of deactivation parameters. However the stability is lower after exposure to moisture.

In contrast, steaming of standard SAPO-34 at 700ºC strongly reduced lifetime. In addition kinetics analysis showed a strong increase in the deactivation parameter.

Therefore, the optimum temperature for an effective stabilization of nanosapo-34 by steaming is 700ºC. From characterization results, this stabilization effect must be related to the migration of single silicon and silicon in the border of the islands with the result of growing these islands with no increase in the population of defects. This migration must have been catalyzed by the presence of water during the steaming, while the decreases in defects (mainly Si-OH groups) are due to annihilation to Si-O-Si and water at high temperature. The decrease in Si in the border of the islands must be produced by combination of different smaller Si islands in single ones.

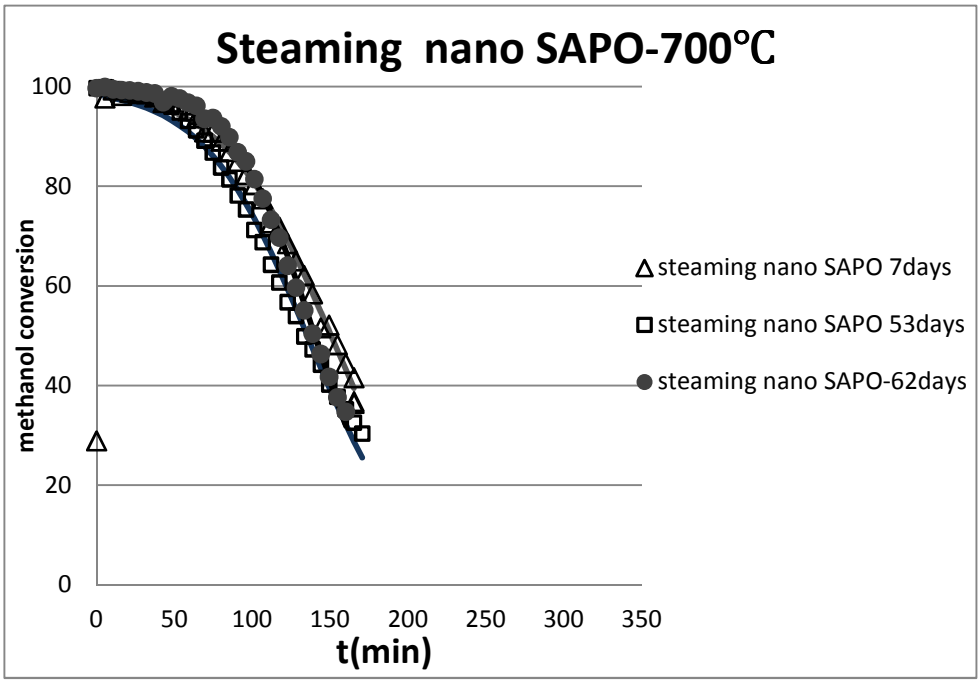

Fig.26 Methanol conversion of steamed nano SAPO-34(700℃)

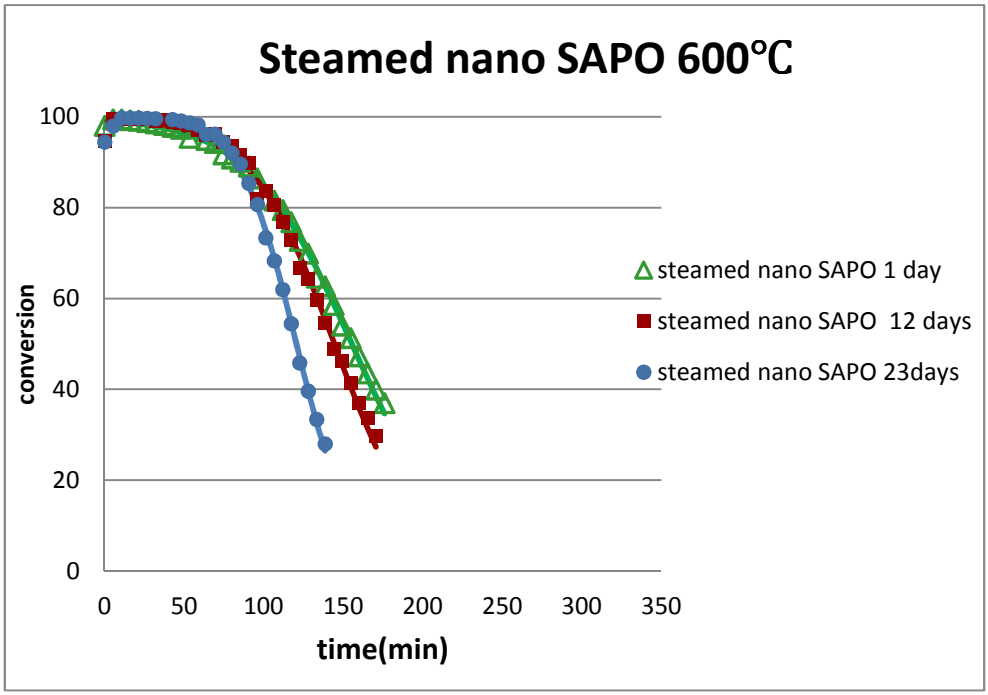

Fig.27 Methanol conversion of steamed Nano SAPO-34(600℃)

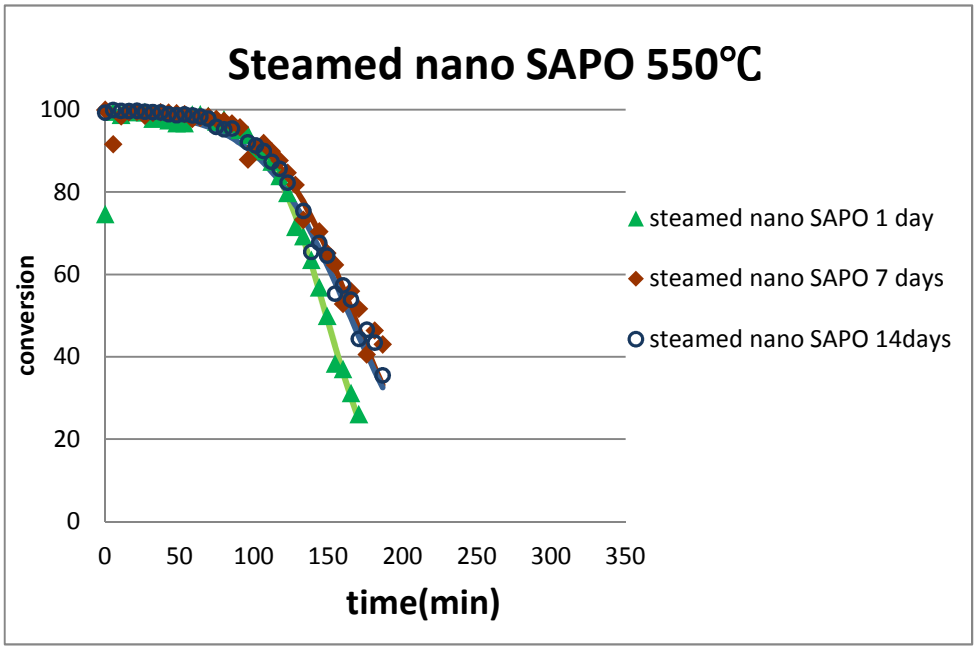

Fig. 28 Methanol conversion of steamed nano SAPO-34(550℃)

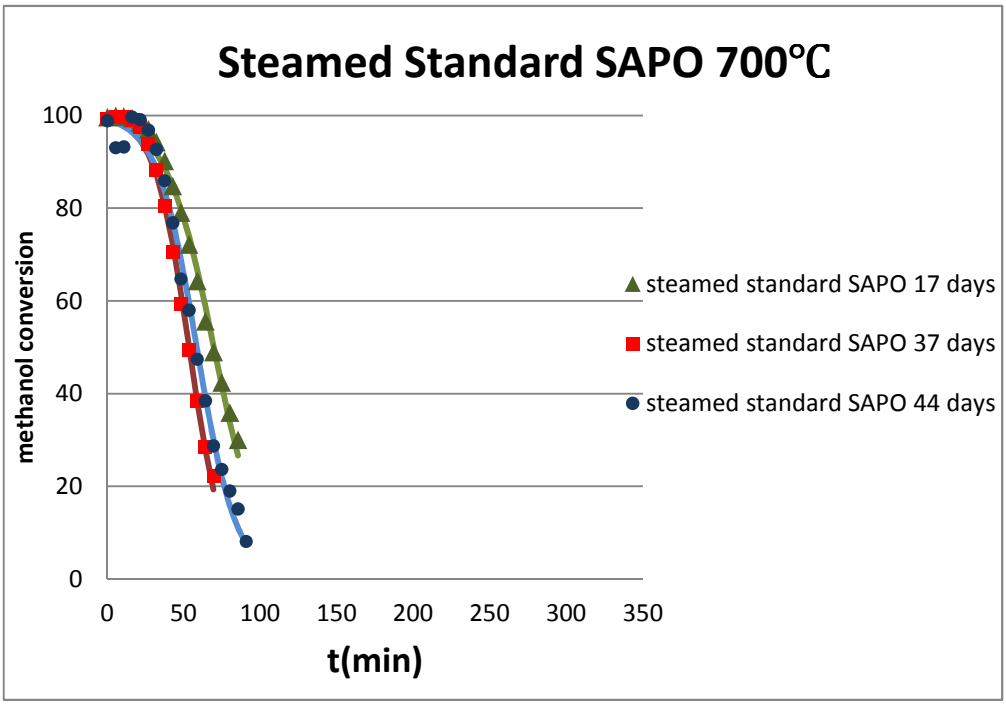

Fig.29 Methanol conversion of steaming Standard SAPO-34

Table 6 the K and a value of steamed nano and standard SAPO-34

Sample: Steaming Nano(700)

days	k	a
7	24.15	0.001199
53	22.60	0.001334
62	29.40	0.001292

Sample: Steaming Nano (600)

days	k	a
1	26.69	0.001162
12	29.91	0.001252
22	37.87	0.001500

Sample: Steaming Nano(550)

days	k	a
1	41.82	0.001217
7	33.79	0.001081
14	29.99	0.001099

Sample: Steaming standard

days	k	a
17	24.76	0.002596
37	26.49	0.003385
44	24.99	0.003093

4. Conclusions

We have shown that nano sized samples of SAPO-34 synthesized by microwave heating presents much higher lifetime than standard SAPO-34 synthesized by conventional hydrothermal method in the reaction of methanol to olefins. However the stability of nanoSAPO-34 to exposure at moisture at room conditions is lower than that of the standard SAPO-34. First, lifetime increased until 14 days of exposure due to the hydrolysis of Si-O-Al bonds of silicon in the border of silicon islands. The acid sites corresponding to these Si species are believed to present higher acidity and favor coking and deactivation of the catalyst. Then, after 14 days, lifetime decreases continuously due to hydrolysis of both Si-O-Al and Al-O-P bonds.

NanoSAPO-34 can be stabilized by steaming at 700ºC 5h. This stabilization

effect is due mainly to the decrease of the population of Silicon species in the border of the Si islands, by migration into these, with subsequent merging of smaller islands into larger ones, and no increase in the relative amount of defects.

The selectivity to different olefins in the reaction strongly changes for samples of nanoSAPO-34 exposed different number of days. The C2/C3 ratio decreases after exposure of the samples to moisture. A higher C_2/C_3 ratio is related to a higher population of Si in the border of the Si islands, with acid sites of higher strength. This is in agreement with a "transition shape selectivity effect" in which higher amount distribution of products is affected by different acid properties of the catalyst and not by merely "easier diffusion" of ethene vs. propene. In addition, the initial olefin distribution is strongly affected by thermodynamical distribution among them, strongly decreasing the yield of ethene, which is produced above the equilibrium by the aromatics-based hydrocarbon pool mechanism.

5. References

1. Corma, A., *Inorganic Solid Acids and Their Use in Acid-Catalyzed Hydrocarbon Reactions.* Chemical Reviews, 1995. **95**(3): p. 559-614.
2. Soler-Illia, G.J.d.A.A., et al., *Chemical Strategies To Design Textured Materials: from Microporous and Mesoporous Oxides to Nanonetworks and Hierarchical Structures.* Chemical Reviews, 2002. **102**(11): p. 4093-4138.
3. Weitkamp, J., *Zeolites and catalysis.* Solid State Ionics, 2000. **131**(1–2): p. 175-188.
4. http://www.iza-structure.org.
5. Song, C., *Selective Conversion of Polycyclic Hydrocarbons to Specialty Chemicals over Zeolite Catalysts.* CATTECH, 2002. **6**(2): p. 64-77.
6. Song, C., et al., *Shape-selective isopropylation of naphthalene over mordenite catalysts: Computational analysis using MOPAC.* Applied Catalysis A: General, 1999. **182**(1): p. 175-181.

7. C. Song, X.M.a.H.H.S., Am. Chem. Soc. Symp. Ser., 1999(738).
8. Boudart, M.D., B. H. Heinemann, H., in *Handbook of Heterogeneous Catalysis*. 2008, Wiley-VCH Verlag GmbH. p. 1-48.
9. Chang, C.D. and A.J. Silvestri, *The conversion of methanol and other O-compounds to hydrocarbons over zeolite catalysts.* Journal of Catalysis, 1977. **47**(2): p. 249-259.
10. Keil, F.J., *Methanol-to-hydrocarbons: process technology.* Microporous and Mesoporous Materials, 1999. **29**(1–2): p. 49-66.
11. Stöcker, M., *Methanol-to-hydrocarbons: catalytic materials and their behavior.* Microporous and Mesoporous Materials, 1999. **29**(1–2): p. 3-48.
12. C.N. Eng, E.C.A., B.V. Vora, *Integration of the UOP/HYDRO MTO process into ethylene plants.* Presented at the 1998 AIChE Spring National Meeting, Session 16, Fundamental Topics in Ethlyene Production, Paper 16g, New Orleans, Louisiana, 1998., 1998.
13. Vora, B.V., et al., *Economic route for natural gas conversion to ethylene and propylene*, in *Studies in Surface Science and Catalysis*, R.L.E.C.P.N.J.H.S. M. de Pontes and M.S. Scurrell, Editors. 1997, Elsevier. p. 87-98.
14. Haw, J.F., et al., *The Mechanism of Methanol to Hydrocarbon Catalysis.* Accounts of Chemical Research, 2003. **36**(5): p. 317-326.
15. Forester, T.R. and R.F. Howe, *In situ FTIR studies of methanol and dimethyl ether in ZSM-5.* Journal of the American Chemical Society, 1987. **109**(17): p. 5076-5082.
16. Murray, D.K., J.W. Chang, and J.F. Haw, *Conversion of methyl halides to hydrocarbons on basic zeolites: a discovery by in situ NMR.* Journal of the American Chemical Society, 1993. **115**(11): p. 4732-4741.
17. Dessau, R.M., *On the H-ZSM-5 catalyzed formation of ethylene from methanol or higher olefins.* Journal of Catalysis, 1986. **99**(1): p. 111-116.
18. Mole, T., G. Bett, and D. Seddon, *Conversion of methanol to hydrocarbons over ZSM-5 zeolite: An examination of the role of aromatic hydrocarbons using 13carbon- and deuterium-labeled feeds.* Journal of Catalysis, 1983. **84**(2): p. 435-445.
19. Langner, B.E., *Reactions of methanol on zeolites with different pore structures.* Applied Catalysis, 1982. **2**(4–5): p. 289-302.
20. Dahl, I.M. and S. Kolboe, *On the reaction mechanism for propene formation in the MTO reaction over SAPO-34.* Catalysis Letters, 1993. **20**(3): p. 329-336.
21. Dahl, I.M. and S. Kolboe, *On the Reaction Mechanism for Hydrocarbon Formation from Methanol over SAPO-34: I. Isotopic Labeling Studies of the Co-Reaction of Ethene and Methanol.* Journal of Catalysis, 1994. **149**(2): p. 458-464.
22. Dahl, I.M. and S. Kolboe, *On the Reaction Mechanism for Hydrocarbon Formation from Methanol over SAPO-34: 2. Isotopic Labeling Studies of the Co-reaction of Propene and Methanol.* Journal of Catalysis, 1996. **161**(1): p. 304-309.
23. Sullivan, R.F., et al., *A New Reaction That Occurs in the Hydrocracking of Certain Aromatic Hydrocarbons.* Journal of the American Chemical Society, 1961. **83**(5): p. 1156-1160.
24. Svelle, S., et al., *Conversion of methanol into hydrocarbons over zeolite H-ZSM-5: Ethene formation is mechanistically separated from the formation of higher alkenes.* JOURNAL OF THE AMERICAN CHEMICAL SOCIETY, 2006. **128**(46): p. 14770-14771.
25. Wu, W., et al., *Dominant reaction pathway for methanol conversion to propene over high silicon H-ZSM-5.* Chemical Engineering Science, 2011. **66**(20): p. 4722-4732.

26. Bjørgen, M., et al., *Conversion of methanol to hydrocarbons over zeolite H-ZSM-5: On the origin of the olefinic species.* Journal of Catalysis, 2007. **249**(2): p. 195-207.
27. Fu, H., W. Song, and J.F. Haw, *Polycyclic Aromatics Formation in HSAPO-34 During Methanol-to-Olefin Catalysis: Ex Situ Characterization After Cryogenic Grinding.* Catalysis Letters, 2001. **76**(1): p. 89-94.
28. Marcus, D.M., et al., *Aromatic Hydrocarbon Formation in HSAPO-18 Catalysts: Cage Topology and Acid Site Density.* Langmuir, 2002. **18**(22): p. 8386-8391.
29. Olsbye, U., et al., *Conversion of Methanol to Hydrocarbons: How Zeolite Cavity and Pore Size Controls Product Selectivity.* Angewandte Chemie International Edition, 2012. **51**(24): p. 5810-5831.
30. Barger, P., *Methanol to olefins (MTO) and beyond*, in *Zeolites for Cleaner Technologies (Catalytic Science Series Vol. 3)*, M. Guisnet and J.P. Gilson, Editors. 2002, Imperial College Press: London. p. 239-260.
31. Yuen, L.T., et al., *Product selectivity in methanol to hydrocarbon conversion for isostructural compositions of AFI and CHA molecular sieves.* Microporous Materials, 1994. **2**(2): p. 105-117.
32. Bleken, F., et al., *The effect of acid strength on the conversion of methanol to olefins over acidic microporous catalysts with the CHA topology.* Topics in Catalysis, 2009. **52**(3): p. 218-228.
33. Park, J.W., et al., *Effects of cage shape and size of 8-membered ring molecular sieves on their deactivation in methanol-to-olefin (MTO) reactions.* Applied Catalysis A: General, 2008. **339**(1): p. 36-44.
34. Zhu, Q., et al., *The study of methanol-to-olefin over proton type aluminosilicate CHA zeolites.* Microporous and Mesoporous Materials, 2008. **112**(1–3): p. 153-161.
35. Shetti, V.N., et al., *Assessment of the mesopore wall catalytic activities of MFI zeolite with mesoporous/microporous hierarchical structures.* Journal of Catalysis, 2008. **254**(2): p. 296-303.
36. C.Q. He, Z.M.L., G.Y. Cai, *Synthesis of Molecular Sieve by Duel-template agent.* Chinese Patent No.ZL94110059.6 1994.
.37. Kim, K.-S., et al., *Vapor Pressures of the 1-Butyl-3-methylimidazolium Bromide+Water,1-Butyl-3-methylimidazolium Tetrafluoroborate+Water, and 1-(2-Hydroxyethyl)-3-methylimidazolium Tetrafluoroborate+Water Systems.* Journal of Chemical & Engineering Data, 2004. **49**(6): p. 1550-1553.
38. Hari Prasad Rao, P.R., et al., *Synthesis of BEA by dry gel conversion and its characterization.* Microporous and Mesoporous Materials, 1998. **21**(4–6): p. 305-313.
39. Lee, Y.J., S.C. Baek, and K.W. Jun, *Methanol conversion on SAPO-34 catalysts prepared by mixed template method.* Applied Catalysis A: General, 2007. **329**: p. 130-136.
40. Wang, P., et al., *The synthesis of SAPO-34 with mixed template and its catalytic performance for methanol to olefins reaction.* Microporous and Mesoporous Materials, 2012. **152**: p. 178-184.
41. Álvaro-Muñoz, T., C. Márquez-Álvarez, and E. Sastre, *Use of different templates on SAPO-34 synthesis: Effect on the acidity and catalytic activity in the MTO reaction.* Catalysis Today, 2012. **179**(1): p. 27-34.
42. Buchholz, A., et al., *Successive steps of hydration and dehydration of silicoaluminophosphates H-SAPO-34 and H-SAPO-37 investigated by in situ CF MAS NMR spectroscopy.* Microporous and Mesoporous Materials, 2003. **57**(2): p. 157-168.
43. Briend, M., et al., *Influence of the Choice of the Template on the Short- and Long-Term Stability of SAPO-34 Zeolite.* J.Phys.Chem., 1995. **99**(20): p. 8270-6.

44. Mees, F.D.P., et al., *Improvement of the hydrothermal stability of SAPO-34.* Chemical Communications, 2003. **9**(1): p. 44-45.
45. Filip Mees, E.V., *Treatment of acid catalysts.* US20030004056, 2003.
46. Filip Mees, E.V., *Treatment of acid catalysts.* US20040157732, 2004.
47. Marcel J. G. Janssen, C.W.M.V.O., Shun C. Fung, Luc R. M. Martens, Wilfried J. Mortier, Ronald G. Searle, Machteld M. Mertens, Stephen N. Vaughn, *Protecting catalytic activity of a SAPO molecular sieve.* US6316683, 1999.
48. Barger, P.T., *Methanol conversion process using SAPO catalysts.* US5095163, 1992.
49. Lin, S., et al., *Fabrication of SAPO-34 crystals with different morphologies by microwave heating.* Topics in Catalysis, 2010. **53**(19-20): p. 1304-1310.
50. Lin, S., et al., *Fabrication of SAPO-34 Crystals with Different Morphologies by Microwave Heating.* Topics in Catalysis, 2010. **53**(19): p. 1304-1310.
51. Buchholz, A., et al., *Thermal stability and dehydroxylation of brønsted acid sites in silicoaluminophosphates H-SAPO-11, H-SAPO-18, H-SAPO-31, and H-SAPO-34 investigated by multi-nuclear solid-state NMR spectroscopy.* Microporous and Mesoporous Materials, 2002. **56**(3): p. 267-278.
52. Blackwell, C.S. and R.L. Patton, *Solid-state NMR of silicoaluminophosphate molecular sieves and aluminophosphate materials.* The Journal of Physical Chemistry, 1988. **92**(13): p. 3965-3970.
53. Lok, B.M., et al., *Silicoaluminophosphate molecular sieves: Another new class of microporous crystalline inorganic solids.* Journal of the American Chemical Society, 1984. **106**(20): p. 6092-6093.
54. Vomscheid, R., et al., *The Role of the Template in Directing the Si Distribution in SAPO Zeolites.* J.Phys.Chem., 1994. **98**(38): p. 9614-18.
55. Martins, G.A.V., et al., *Revisiting the nature of the acidity in chabazite-related silicoaluminophosphates: Combined FTIR and29Si MAS NMR study.* Journal of Physical Chemistry C, 2007. **111**(1): p. 330-339.
56. Wei, Y., et al., *Synthesis, characterization and catalytic performance of metal-incorporated SAPO-34 for chloromethane transformation to light olefins.* Catalysis Today, 2008. **131**(1–4): p. 262-269.
57. Xu, L., et al., *Synthesis of SAPO-34 with only Si(4Al) species: Effect of Si contents on Si incorporation mechanism and Si coordination environment of SAPO-34.* Microporous and Mesoporous Materials, 2008. **115**(3): p. 332-337.
58. Prakash, A.M. and S. Unnikrishnan, *Synthesis of SAPO-34: High silicon incorporation in the presence of morpholine as template.* Journal of the Chemical Society, Faraday Transactions, 1994. **90**(15): p. 2291-2296.
59. Suzuki, K., et al., *Ammonia IRMS-TPD measurements on Brønsted acidity of proton-formed SAPO-34.* Physical Chemistry Chemical Physics, 2011. **13**(8): p. 3311-3318.
60. Katada, N., et al., *Acidic properties of cage-based, small-pore zeolites with different framework topologies and their silicoaluminophosphate analogues.* Journal of Physical Chemistry C, 2011. **115**(45): p. 22505-22513.
61. Sastre, G., et al., *Modeling of silicon substitution in SAPO-5 and SAPO-34 molecular sieves.* Journal of Physical Chemistry B, 1997. **101**(27): p. 5249-5262.
62. Barthomeuf, D., *Topological model for the compared acidity of SAPOs and SiAl zeolites.* Zeolites, 1994. **14**(6): p. 394-401.

63. Buchholz, A., et al., *Sequential Steps of Ammoniation of the Microporous Silicoaluminophosphates H-SAPO-34 and H-SAPO-37 Investigated by In Situ CF MAS NMR Spectroscopy.* Journal of Physical Chemistry B, 2004. **108**(10): p. 3107-3113.
64. Watanabe, Y., et al., *Multinuclear NMR Studies on the Thermal Stability of SAPO-34.* Journal of Catalysis, 1993. **143**(2): p. 430-436.
65. Busca, G., et al., *FT-113 study of the surface properties of the spinels NiAl2O4 and CoAl2O4 in relation to those of transitional aluminas.* Journal of Catalysis, 1991. **131**(1): p. 167-177.
66. Busca, G., et al., *Surface sites on spinel-type and corundum-type metal oxide powders.* Langmuir, 1993. **9**(6): p. 1492-1499.
67. Eilertsen, E.A., et al., *Single parameter synthesis of high silica CHA zeolites from fluoride media.* MICROPOROUS AND MESOPOROUS MATERIALS, 2012. **153**(0): p. 94-99.
68. Gianotti, E., et al., *Acidity of mesoporous aluminophosphates and silicas MCM-41. A combined FTIR and UV-Vis-NIR study*, in *STUDIES IN SURFACE SCIENCE AND CATALYSIS*, G.G. R. Aiello and F. Testa, Editors. 2002, Elsevier. p. 1419-1426.
69. Bordiga, S., et al., *Assessing the acidity of high silica chabazite H-SSZ-13 by FTIR using CO as molecular probe: Comparison with H-SAPO-34.* JOURNAL OF PHYSICAL CHEMISTRY B, 2005. **109**(7): p. 2779-2784.
70. Janssens, T.V.W., *A new approach to the modeling of deactivation in the conversion of methanol on zeolite catalysts.* Journal of Catalysis, 2009. **264**(2): p. 130-137.
71. Zhou, H., et al., *Kinetics of the reactions of the light alkenes over SAPO-34.* Applied Catalysis A: General, 2008. **348**(1): p. 135-141.
72. Chen, D., et al., *Influence of Coke Deposition on Selectivity in Zeolite Catalysis.* Ind.Eng.Chem.Res., 1997. **36**(9): p. 3473-3479.
73. Sedran, U., A. Mahay, and H.I. De Lasa, *Modelling methanol conversion to hydrocarbons: revision and testing of a simple kinetic model.* Chemical Engineering Science, 1990. **45**(5): p. 1161-1165.
74. Chen, D., et al., *The role of coke deposition in the conversion of methanol to olefins over SAPO-34.* Stud.Surf.Sci.Catal., 1997. **111**(Catalyst Deactivation 1997): p. 159-166.
75. Chen, D., et al., *Methanol Conversion to Light Olefins over SAPO-34 - Sorption, Diffusion, and Catalytic Reactions.* INDUSTRIAL & ENGINEERING CHEMISTRY RESEARCH, 1999. **38**(11): p. 4241-4249.
76. Svelle, S., et al., *How defects and crystal morphology control the effects of desilication.* CATALYSIS TODAY, 2011. **168**(1): p. 38-47.
77. Sazama, P., et al., *FTIR and 27Al MAS NMR analysis of the effect of framework Al- and Si-defects in micro- and micro-mesoporous H-ZSM-5 on conversion of methanol to hydrocarbons.* Microporous and Mesoporous Materials, 2011. **143**(1): p. 87-96.
78. Chen, D., et al., *Methanol Conversion to Light Olefins over SAPO-34: Reaction Network and Deactivation Kinetics.* Industrial & Engineering Chemistry Research, 2006. **46**(12): p. 4116-4123.
79. Dahl, I.M., et al., *Structural and chemical influences on the MTO reaction: a comparison of chabazite and SAPO-34 as MTO catalysts.* Microporous Mesoporous Mater., 1999. **29**(1-2): p. 185-190.
80. Hereijgers, B.P.C., et al., *Product shape selectivity dominates the Methanol-to-Olefins (MTO) reaction over H-SAPO-34 catalysts.* Journal of Catalysis, 2009. **264**(1): p. 77-87.
81. Song, W., H. Fu, and J.F. Haw, *Supramolecular Origins of Product Selectivity for Methanol-to-Olefin Catalysis on HSAPO-34.* Journal of the American Chemical Society, 2001. **123**(20): p. 4749-4754.

82. Arstad, B., J.B. Nicholas, and J.F. Haw, *Theoretical Study of the Methylbenzene Side-Chain Hydrocarbon Pool Mechanism in Methanol to Olefin Catalysis.* Journal of the American Chemical Society, 2004. **126**(9): p. 2991-3001.